High-Resolution Solution Structure of the EGF-like Domain of Heregulin-α‡

Neil E. Jacobsen,§,|| Nasrin Abadi,⊥ Mark X. Sliwkowski,⊥ Dorothea Reilly,# Nicholas J. Skelton,§ and Wayne J. Fairbrother*,§

Departments of Protein Engineering, Protein Chemistry, and Cell Culture, Genentech, Inc., 460 Point San Bruno Boulevard, South San Francisco, California 94080

Received November 6, 1995; Revised Manuscript Received December 14, 1995⊗

ABSTRACT: The solution structure of the 63-residue heregulin-α (HRG-α) epidermal growth factor (EGF)-like domain, corresponding to residues 177−239 of HRG-α, has been determined to high resolution using data from two-dimensional and three-dimensional homo- and heteronuclear NMR spectroscopy. The structure is based on a total of 887 internuclear distance and dihedral restraints derived from data obtained using unlabeled and uniformly ^{15}N-labeled protein samples, at pH 4.5, 20 °C. A total of 20 structures were calculated using a hybrid distance geometry−simulated annealing approach with the program DGII, followed by restrained molecular dynamics using the program DISCOVER. The average maximum violations are 0.12 ± 0.01 Å and 1.4 ± 0.3° for distance and dihedral restraints, respectively. The backbone (N, C^{α}, C) atomic rms distribution about the mean coordinates for residues 3−23 and 31−49 is 0.29 ± 0.07 Å. The N- and C-terminal residues (1−2 and 50−63) and the Ω-loop comprising residues 24−30 are disordered. Comparison of the HRG-α EGF-like domain structure with the previously determined structure of human EGF [Hommel et al. (1992) *J. Mol. Biol. 227*, 271−282] reveals a high degree of structural similarity; excluding the N-terminal region (residues 1−13), the disordered Ω-loop region (residues 24−30) that contains a three-residue insertion in HRG-α relative to hEGF, and the disordered C-terminal region (residues 50−63), the C^{α} alignment between the HRG-α and hEGF minimized mean structures has a rms difference of ∼1 Å. In HRG-α the N-terminal residues 2−6 form a well-defined β-strand rather than being disordered as found for hEGF. This structural difference correlates with functional data which suggest that the N-terminal region of the HRG-α EGF-like domain is responsible for the observed receptor specificity differences between HRG-α and EGF.

The epidermal growth factor receptor (EGFR) family of receptor tyrosine kinases consists of four members: EGFR and *Erb*B-2, -3, and -4. Ligands for EGFR include EGF, TGF-α, amphiregulin, HB-EGF, betacellulin, and several pox virus gene products. Sequence identity among this family of growth factors is 30−45%; EGF or TGF-α bind only to EGFR, however, and not to any of the other receptor family members (Groenen et al., 1994; Modjtahedi & Dean, 1994). More recently a second family of proteins, known as neuregulins, has been identified (Mudge, 1993; Hynes & Stern, 1994). Unlike the members of the EGFR ligand family which are different gene products, neuregulins arise from alternative splicing of mRNA encoded by a single gene that has been localized to human chromosome 8p22-p11 (Lee & Wood, 1993; Orr-Urtreger et al., 1993). Although *Erb*B-3 and *Erb*B-4 serve as receptors for neuregulins, transactivation of *Erb*B-2 is frequently encountered as a consequence of neuregulin interaction with these receptors (Carraway & Cantley, 1994; Earp et al., 1995). Indeed, the initial isolation of two of these ligands, heregulin (HRG) (Holmes et al., 1992) and neu differentiation factor (NDF) (Peles et al., 1992), was accomplished by monitoring the stimulation of *Erb*B-2 tyrosine phosphorylation that occurred on breast tumor cell lines as a result of HRG or NDF treatment. Independently, two other closely related biological activities that occur at the neural-Schwann cell (Marchionni et al., 1993) and the neuromuscular (Falls et al., 1993) interfaces were also identified and are now known to be neuregulin gene products. Expression of a particular neuregulin isoform appears to be tissue specific (Meyer & Birchmeier, 1994; Ho et al., 1995); one feature that all of the isoforms have in common, however, is the presence of a single EGF-like domain within a multimotif structure. The EGF-like domain of HRG binds with similar affinities to *Erb*B-3 or *Erb*B-4 (Tzahar et al., 1994) and is sufficient to mediate all the known biological activities including the stimulation of breast and ovarian tumor cell growth (Lewis et al., 1995), Schwann cell growth (Levi et al., 1995), and the induction of the ϵ-subunit of the acetylcholine receptor (Altiok et al., 1995; Chu et al., 1995; Moscoso et al., 1995).

Clinical interest in this family of growth factor receptors stems from the fact that they are frequently overexpressed in a number of human cancers (Hynes & Stern, 1994; Modjtahedi & Dean, 1994). In some instances the overexpression of these receptors or their ligands has been correlated with poor clinical outcome (Hynes, 1993). Thus, these receptors and perhaps their ligands may be viewed as potential therapeutic targets for the development of drugs that interfere with receptor activation (Baselga & Mendelsohn, 1994). The two newer members of this family, *Erb*B-3 and *Erb*B-4, have not been studied in as much detail as

‡ Coordinates for the minimized mean and final ensemble of structures have been deposited in the Brookhaven Protein Data Bank under the file names 1HAF and 1HAE, respectively.

* To whom correspondence should be addressed.

§ Department of Protein Engineering.

|| Present address: Department of Chemistry, University of Arizona, Tucson, AZ 85721.

⊥ Department of Protein Chemistry.

Department of Cell Culture.

⊗ Abstract published in *Advance ACS Abstracts,* February 1, 1996.

0006-2960/96/0435-3402$12.00/0

EGFR and *Erb*B-2. *Erb*B-4 is a fully functional HRG receptor whose precise role in mediating HRG responsiveness in biologically relevant systems is unknown (Plowman et al., 1993a,b). *Erb*B-3 has been found to be expressed in a significant number of breast (Lemoine et al., 1992a) and pancreatic tumors (Lemoine et al., 1992b). At present HRG-mediated signaling through *Erb*B-3 is thought to require co-expression of an additional receptor tyrosine kinase, since the intrinsic tyrosine kinase activity of *Erb*B-3 appears to be severely impaired (Guy et al., 1994; Kim et al., 1994). In model systems, coexpression of *Erb*B-3 with *Erb*B-2 reconstitutes a high-affinity HRG receptor that is a very active receptor complex (Sliwkowski et al., 1994). Recently, it has been demonstrated that the oncogenic potential of *Erb*B-3 and *Erb*B-2 is much greater than either receptor alone in causing fibroblast transformation (Alamandi et al., 1995; Wallasch et al., 1995). Responsiveness of breast and ovarian tumor cells to HRG also appears to be mediated by an interaction with a receptor complex involving *Erb*B-2 (Graus-Porta et al., 1995; Lewis et al., 1995).

We report here the determination of the high-resolution solution structure of the 63-residue EGF-like domain, corresponding to residues 177−239 of native HRG-α (Holmes et al., 1992). For convenience, we chose to number the residues in this HRG-α domain sequentially from 1 to 63. The use of uniformly ^{15}N-labeled recombinant protein and 3D heteronuclear NMR spectroscopy has resulted in the determination of significantly more internuclear distance and dihedral angle restraints than was possible for a previous structure determination of this domain using an unlabeled synthetic protein and 2D homonuclear NMR techniques (Nagata et al., 1994). As a consequence, the present structure is both more precise and more accurate than that previously reported. Indeed, structural comparisons reveal that the new structure more closely resembles that of hEGF (Hommel et al., 1992) than the structure of Nagata et al. (1994). Detailed comparison of the new high-resolution structure with the previously determined structures of hEGF (Hommel et al., 1992) and hTGF-α (Harvey et al., 1991) can be correlated with the results of existing (Barbacci et al., 1995) and future functional studies to give an improved understanding of the receptor specificity differences between these different proteins.

MATERIALS AND METHODS

Expression and Purification of the HRG-α EGF-like Domain. The expression vector for the HRG-α EGF-like domain (residues 177−239 of native HRG-α) was described previously (Holmes et al., 1992) and is designed to direct secretion of the protein into the periplasmic space of *Escherichia coli*. Protein purification was performed by osmotically shocking *E. coli* cells in 50 mM Tris-HCl, pH 8, buffer containing 5 mM EDTA and 5 mM EGTA and the protease inhibitors pepstatin A, PMSF, and aprotinin. Release of the HRG-α EGF-like domain from the pepriplasm was assisted by sonication with a probe sonicator. Intact cells and debris were separated from the released proteins by centrifugation at 15000 *g* for 15 min. The resulting supernatant was purified by ultrafiltration on a YM-30 (Amicon). Retained proteins were discarded, and the ultrafiltrate was applied to a Fast Flow Q (Pharmacia) anion-exchange column that had been previously equilibrated with 50 mM Tris-HCl, pH 8, buffer. The flow-through from this anion-exchange column was adjusted to approximately pH 2 with TFA and applied to a C4 reversed-phase column (Vydac 214TP152022; 2.2 × 25 cm) which had been equilibrated in 0.095% TFA in H_2O. The C4 column was eluted with a linear 0.095 % TFA/CH_3CN gradient, with the HRG-α EGF-like domain eluting at ∼20% CH_3CN. Further purification of HRG-α was accomplished by 20% isocratic elution from a reversed-phase C4 column (Vydac C4R103-25; 0.46 × 25 cm). This final chromatography step was used to enrich for the HRG-α EGF-like domain that did not contain oxidized methionine residues. The final yield of protein obtained using this protocol was ∼35 mg/L of starting culture from a 10 L fermentor.

Production of the uniformly ^{15}N-labeled HRG-α EGF-like domain was performed essentially as described (Reilly & Fairbrother, 1994). Shake flask fermentation of the ^{15}N-labeled protein resulted in different expression levels and a more complex contaminating protein profile; additional purification procedures were therefore employed. *E. coli* cell shockates were prepared as described above, the resulting supernatant was adjusted to pH 3.4 with H_3PO_4, and urea was added to a final concentration of 4 M. This solution was applied to a Fast Flow S cation-exchange column that was equilibrated in 25 mM NaH_2PO_4, pH 3.4, buffer containing 4 M urea. After sample application the column was washed with several column volumes of equilibration buffer and then eluted with the same buffer containing 0.2 M NaCl followed by a 0.6 M NaCl elution. The HRG-α EGF-like domain was found in the 0.6 M eluate, and this solution was then diluted with 2 parts of 4 M urea in 25 mM NaH_2PO_4, pH 3.4, buffer, giving a final NaCl concentration of 0.2 M. This solution was applied to a Mono S (Pharmacia; HR 5/5) column that had been previously equilibrated with 25 mM NaH_2PO_4, pH 3.4, buffer containing 4 M urea. This column was developed with a NaCl gradient to 1 M NaCl. The HRG-α EGF-like domain eluted between 0.30 and 0.35 M NaCl. These fractions were concentrated on a YM-3 (Amicon) ultrafiltration membrane and then applied to a Superdex 75 (Pharmacia; 16/20) equilibrated in 25 mM NaH_2PO_4, pH 3.4, buffer containing 6 M Gdn-HCl. Desalting and final purification of the ^{15}N-labeled HRG-α EGF-like domain was accomplished by reversed-phase HPLC as described above. The final yield of ^{15}N-labeled protein obtained using this procedure was ∼11 mg/L of starting culture.

Disulfide Bond Mapping. The HRG-α EGF-like domain was digested with trypsin (Promega) at an enzyme-to-substrate ratio of 1:20 for 16 h at room temperature in 0.1 M NH_4HCO_3 buffer, pH 7.8. The resulting peptides were then purified by reversed-phase HPLC using a C4 column (Synchropak 100; 0.46 × 10 cm). Peptides eluting at ∼29 and ∼38 min were found to contain the T7 + T8 and the T2 + T4 + T6 peptides, respectively (Table 1). To assign the disulfide pattern of the T2 + T4 + T6 peptide, this peptide was further digested with V8 protease (Boehringer Mannheim) at an enzyme-to-substrate ratio of 1:5 for 30 h at 37 °C in 0.05 M NH_4HCO_3 buffer, pH 7.8. The resulting peptides were resolved on a C18 column (Alltech; 0.21 × 10 cm). Peptide identification was made by mass spectrometry and in some instances verified by automated Edman N-terminal sequence analysis or amino acid compositional analysis.

Sample Preparation. NMR samples were prepared in 90% H_2O/10% D_2O solution (50 mM sodium acetate-d_3, pH 4.5, 1.0 mM NaN_3). Final protein concentrations were 1.4 and

Table 1: Disulfide Mapping of Heregulin-α

		theoretical mass	observed mass
tryptic digest of HRG-α			
T2 (6−9)	CAEK		
T4 (12−24)	TFCVNGGECFMVK	2405.9	2405.9 ± 0.3
T6 (32−35)	YLCK		
T7 (36−44)	CQPGFTGAR	1855.1	1854.5 ± 0.5
T8 (45−52)	CTENVPMK		
V8 digest of T2−T4−T6			
T2 (6−9)	CAEK	1074.3	1073.8 ± 0.4
T4V2 (20−24)	CFMVK		
T4V1 (12−19)	TFCVNGGE	1349.5	1349.2 ± 0.0
T6 (32−35)	YLCK		

3.8 mM for the unlabeled and uniformly ^{15}N-labeled samples, respectively. A D_2O sample was prepared by lyophilizing the unlabeled 90% H_2O sample and dissolving the residue in 500 μL of D_2O/acetic acid-d_3 (27.3 mM). The amount of acetic acid was estimated to replace that lost from the buffer during lyophilization. The chemical shift of $^1H^{\epsilon 1}$ of the single histidine residue was unchanged from its value in H_2O, indicating that the apparent pH remained unchanged; subsequent measurement of the pH confirmed this to be the case.

NMR Spectroscopy. All spectra were acquired at either 20 or 30 °C on a Bruker AMX-500 spectrometer with a 5 mm triple-resonance ($^1H/^{15}N/^{13}C$) probe. Proton chemical shifts were referenced to internal sodium 3-(trimethylsilyl)-1-propanesulfonate (TPS). The ^{15}N chemical shifts were referenced indirectly to liquid NH_3 (Live et al., 1984).

The following homonuclear 2D NMR spectra were recorded using standard pulse sequences and phase cycling: DQF-COSY (Rance et al., 1983), double-quantum (2Q) (Braunschweiler et al., 1984; Rance & Wright, 1986), TOCSY (Braunschweiler & Ernst, 1983; Bax & Davis, 1985), NOESY (Kumar et al., 1980; Bodenhausen et al., 1984), jump-and-return NOESY (Plateau & Guéron, 1982), and TOCSY-relayed NOESY (Rance, 1987; Kessler et al., 1988). All homonuclear 2D spectra were acquired in the phase-sensitive mode using time-proportional phase incrementation (TPPI) for quadrature detection in the t_1 dimension (Marion & Wüthrich, 1983). Spectra were typically acquired with 4096 complex points in t_2 and an F_2 spectral width of 12.5 kHz; 750 real points were typically acquired in t_1 with an F_1 spectral width of 6250 Hz. With the exception of the JR-NOESY experiments the solvent signal was suppressed by low-power phase-locked presaturation for 1.5 s. For spectra acquired in 90% H_2O, the solvent signal was further attenuated by convolution difference in t_2 (Marion et al., 1989b).

Double-quantum spectra were acquired with a total preparation delay of 32 ms and spectral widths of 8000 and 6250 Hz in F_1 and F_2, respectively. TOCSY, NOESY, JR-NOESY, and TOCSY-relayed NOESY spectra were each acquired with the normal pulse sequences followed by a short Hahn-echo period to improve the quality of both the solvent suppression and the baseline (Rance & Byrd, 1983; Davis, 1989). TOCSY spectra were acquired using a 70 ms "clean" DIPSI-2rc isotropic mixing sequence (Cavanagh & Rance, 1992). NOESY spectra were acquired with mixing times of 50 and 100 ms; solvent was irradiated during the mixing time for 90% H_2O samples. JR-NOESY spectra were acquired with mixing times of 150 and 200 ms. The TOCSY-relayed NOESY sequence was identical to the NOESY sequence except that a 34 ms DIPSI-2rc mixing period was inserted prior to the 100 ms NOESY mixing period.

A homonuclear 3D NOESY-TOCSY spectrum of the unlabeled sample in D_2O solution was also acquired at 20 °C as an aid in the assignment of ambiguous 2D NOE cross peaks (Vuister et al., 1988, 1989, 1990). The NOESY mixing time was 100 ms and the TOCSY isotropic (DIPSI-2rc) mixing time was 45 ms. Spectral widths were 4200 Hz in t_1 and t_2 and 6250 Hz in t_3. Quadrature detection in the t_1 and t_2 dimensions was achieved using the TPPI−States method (Marion et al., 1989c). The acquired data matrix comprised 128 (t_1) × 128 (t_2) × 512 (t_3) complex data points. Zero-filling and linear prediction were employed to yield a final absorptive spectrum of 256 (F_1) × 256 (F_2) × 512 (F_3) points.

3D ^{1}H−^{15}N TOCSY-HSQC and NOESY-HSQC spectra (Marion et al., 1989a,d; Driscoll et al., 1990; Fesik & Zuiderweg, 1990) of ^{15}N-labeled protein were acquired at 20 °C using spin-lock purge pulses for solvent suppression (Messerle et al., 1989). The DIPSI-2rc sequence was used for ^{1}H isotropic mixing in the TOCSY-HSQC experiment; spectra were acquired with isotropic mixing times of 29 and 70 ms. A single NOESY-HSQC spectrum was acquired with a mixing time of 100 ms. The spectra were recorded in the pure absorption mode using TPPI for quadrature detection in both the t_1 and t_2 dimensions. Low-power GARP-1 phase modulation (Shaka et al., 1985) was used for ^{15}N decoupling during acquisition. The acquired data matrices for each 3D experiment were 256 real (t_1) × 64 real (t_2) × 1024 complex (t_3) data points, with spectral widths of 4980, 977.7, and 6250 Hz in the F_1(^{1}H), F_2(^{15}N), and F_3($^1H^N$) dimensions, respectively. Zero-filling and linear prediction were employed to yield final spectra of 512 (F_1) × 64 (F_2) × 1024 (F_3) points.

$^3J_{H^N-H^\alpha}$ coupling constants were determined from either a high digital resolution DQF-COSY spectrum, using the Levenberg−Marquardt algorithm (Press et al., 1986) to fit the antiphase double-Lorentzian F_2 cross sections of resolved $^1H^N-^1H^\alpha$ cross peaks, or from a 3D HNHA spectrum of the ^{15}N-labeled sample (Vuister & Bax, 1993). The 3D HNHA experiment was acquired using the TPPI−States method for quadrature detection in both the t_1 and t_2 dimensions. The acquired data matrix was 32 (t_1) × 64 (t_2) × 1024 (t_3) complex data points, with spectral widths of 977.7, 4980, and 6250 Hz in the F_1(^{15}N), F_2(^{1}H), and F_3($^1H^N$) dimensions, respectively. Zero-filling and linear prediction were employed to yield a final spectrum of 64 (F_1) × 256 (F_2) × 1024 (F_3) points. The apparent coupling constants obtained from the cross peak to diagonal intensity ratios in the HNHA spectrum were increased by 10% to correct for the effects of $^1H^\alpha$ relaxation. The 10% correction factor was determined empirically by comparing coupling constants measured for well-resolved cross peaks in the DQF-COSY spectrum with the equivalent coupling constants determined from well-resolved peaks in the HNHA spectrum. This value is greater than might be expected for a 63-residue protein (it is comparable to the value of 11% used previously for SNase, a 141-residue protein), suggesting that the 3.8 mM solution

of the ^{15}N-labeled HRG-α EGF-like domain may be aggregated. Subsequent relaxation measurements have confirmed this to be the case (W. J. Fairbrother, unpublished results).

A constant-time HNHB spectrum (Archer et al., 1991) was acquired in order to obtain qualitative estimates of the magnitude of the $^3J_{N-H^\beta}$ coupling constants. The TPPI−States method was used for quadrature detection in both the t_1 and t_2 dimensions. The acquired data matrix was 32 (t_1) × 64 (t_2) × 1024 (t_3) complex data points, with spectral widths of 977.7, 4980, and 6250 Hz in the F_1(^{15}N), F_2(^{1}H), and F_3($^1H^N$) dimensions, respectively. The use of zero-filling and linear prediction yielded a final spectrum of 64(F_1) × 256(F_2) × 1024(F_3) points.

Amide hydrogen/deuterium exchange kinetics were monitored at 20 °C using a fast TOCSY experiment (Marion et al., 1989c) with a 33 ms mixing time, a spectral width of 2864 Hz in F_1, and a final t_1 delay of 45 ms. A series of such spectra were acquired starting immediately following dissolution of the lyophilized protein sample in ice-chilled D_2O/acetic acid-d_3 (as described above); a total experiment time of 34 min was used for the first five experiments, 68 min for the next four, and 136 min for the final two. Each set of fast TOCSY data was transformed into a 1024 × 512 matrix, discarding the first 2400 points in F_2 and the first 300 points in F_1. Cross-peak volumes (scaled according to the total acquisition time) were plotted as a function of time at the midpoint of each experiment and fit to an exponential decay equation with three coefficients to determine the decay rate. Protection factors were determined using intrinsic amide exchange rates corrected for pH and temperature (Molday et al., 1972; Englander et al., 1979; Robertson & Baldwin, 1991).

All spectra were processed and analyzed on Silicon Graphics workstations using the program FELIX (Biosym Technologies, Inc., San Diego).

Distance and Dihedral Angle Restraints. Interproton distance restraints were derived from assigned NOE cross peaks in the 3D ^{1}H−^{15}N NOESY-HSQC and 2D homonuclear NOESY spectra of the ^{15}N-labeled and unlabeled D_2O samples, respectively, acquired at 20 °C with mixing times of 100 ms. Cross peaks in the D_2O NOESY were classified as very strong, strong, medium, or weak on the basis of integrated volumes and assigned upper distance bounds of 2.7, 3.3, 4.2, or 5.5 Å. Cross peaks in the 3D NOESY-HSQC spectrum were similarly classified as very strong, strong, medium, weak, or very weak, corresponding to upper distance bounds of 2.7, 3.3, 4.2, 5.0, and 6.5 Å. The latter category includes very weak cross peaks that were not observed in the 2D H_2O NOESY spectrum and accounts for spin diffusion present in the 3D NOESY-HSQC spectrum of the more concentrated ^{15}N-labeled sample. The upper bound distance restraints assigned to overlapped cross peaks were either increased by one category relative to their integrated volumes or set to the maximum upper bound, depending on a qualitative assessment of the severity of the overlap. The integrated volumes of cross peaks involving methyl or degenerate methylene protons, and protons of rapidly flipping aromatic side chains, were divided by the number of protons contributing to the resonance prior to distance categorization (Yip, 1990). Lower distance bounds between nonbonded protons were set to the sum of their van der Waals radii. Pseudoatom corrections were added to the upper bound distance restraints where necessary (Wüthrich et al., 1983). A 0.5 Å correction was added to the upper bound for methyl protons (Tropp, 1980; Koning et al., 1990). Where appropriate, $\langle r^{-6}\rangle$ averaging was applied to restraints involving nonstereospecifically assigned methylene protons or the protons of rapidly flipping aromatic side chains (Brünger et al., 1986; Clore et al., 1986).

ϕ dihedral angle restraints were derived from $^3J_{H^N-H^\alpha}$ coupling constants measured directly from a high digital resolution DQF-COSY spectrum or obtained from a 3D HNHA spectrum (see above). The ϕ angle was restrained to between −150° and −90° for $^3J_{H^N-H^\alpha} > 8$ Hz and to between −80° and −50° for $^3J_{H^N-H^\alpha} < 5$ Hz. Additional ϕ angle restraints, between −180° and −20°, were applied to residues for which the intraresidue $^1H^\alpha-^1H^N$ NOE was clearly weaker than the sequential $^1H^\alpha-^1H^N$ NOE from the preceding residue (Clubb et al., 1994). Stereospecific assignments of β-methylene protons and χ_1 dihedral angle restraints were derived from qualitative estimates of the magnitudes of the $^3J_{H^\alpha-H^\beta}$ and $^3J_{N-H^\beta}$ coupling constants obtained from 3D ^{1}H−^{15}N TOCSY-HSQC (29 ms mixing time) and HNHB spectra, respectively, together with the results from preliminary structure calculations (Wagner et al., 1987; Montelione et al., 1989; Clore et al., 1991). The minimum range employed for the χ_1 dihedral angle restraints was ±30°.

Hydrogen bond restraints were based upon observation of slow amide proton−solvent exchange and characteristic sequential and long-range NOEs involving $^1H^N$ and $^1H^\alpha$. Hydrogen bond restraints were included only if a hydrogen bond was observed in greater than 50% of the lowest energy structures resulting from initial structure calculations performed in the absence of such restraints. Each hydrogen bond identified was defined using two distance restraints: r_{NH-O} = 1.8−2.2 Å and r_{N-O} = 2.7−3.3 Å.

Structure Calculations. Structures were calculated using a hybrid distance geometry−dynamical simulated annealing protocol (Nilges et al., 1988), followed by energy refinement using restrained molecular dynamics (rMD). Distance geometry calculations were performed using the program DG-II (Havel, 1991) within the INSIGHT II package (Biosym Technologies, Inc., San Diego). Following triangle bounds smoothing, distance matrices that satisfied the triangle inequality limits were generated using random metrization, and coordinates satisfying the trial distances were obtained by prospective embedding and majorization in four dimensions. The embedded structures were then optimized by simulated annealing in four dimensions and conjugate gradient minimization in three dimensions (Havel, 1991) using the CVFF parameters (Biosym Technologies, Inc., San Diego). Eighty-eight structures successfully converged of 100 embeds attempted.

The top 50 distance geometry structures (those with the lowest total penalty function) were further subjected to two rounds of rMD using the program DISCOVER, modified to include $\langle r^{-6}\rangle$ averaging (Biosym Technologies, Inc., San Diego). The all-atom AMBER force field (Weiner et al., 1984, 1986) was used, with a 12.0 Å cutoff for nonbonded interactions and a distance-dependent dielectric constant, $\epsilon = 4r$, to compensate for the lack of explicit solvent. Side-chain partial atomic charges on Asp, Glu, Arg, and Lys residues were reduced to give total charges of ±0.2 in order to reduce artifacts due to charge−charge interactions. Each structure was initially minimized using 100 steps of steepest descents minimization, followed by 1000 steps of conjugate

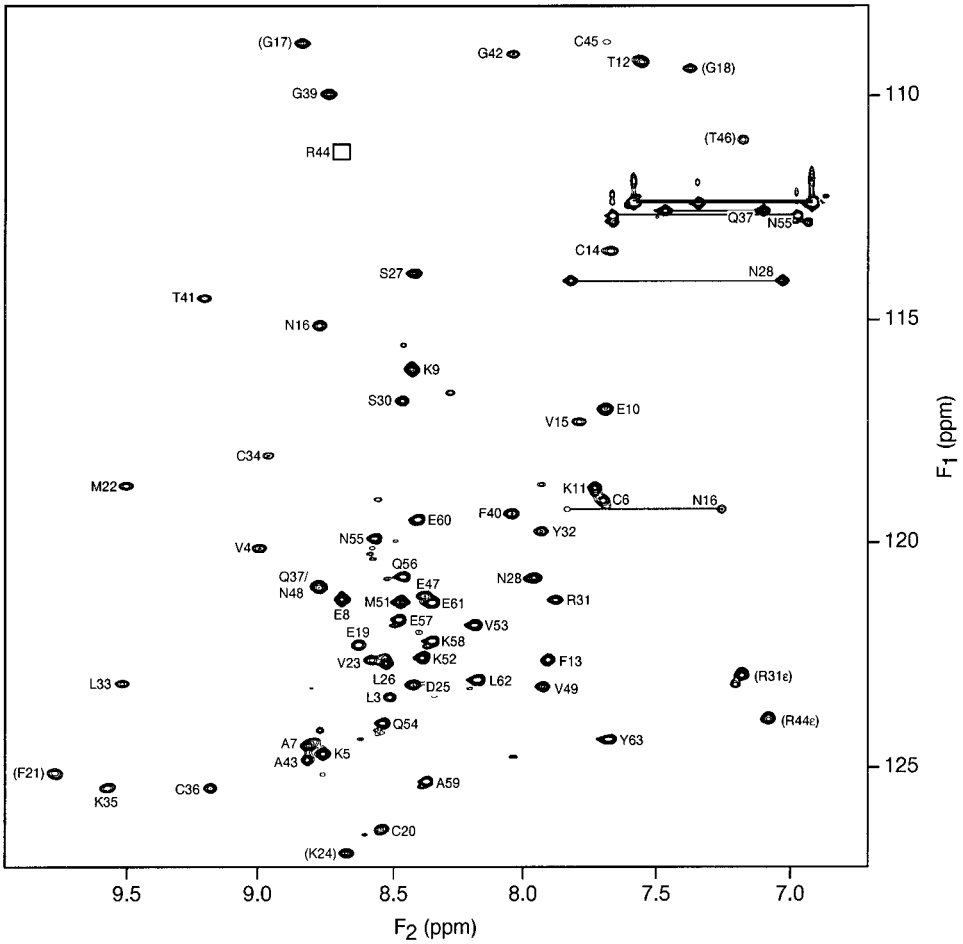

FIGURE 1: $^1H-^{15}N$ HSQC spectrum of the ^{15}N-labeled HRG-α EGF-like domain recorded using TPPI for quadrature detection in t_1. The assignments obtained in this study are indicated. Assignments in parentheses indicate cross peaks that have been folded in F_1 (actual chemical shifts are listed in supporting information, Table S1). The cross peak for Arg44 is broad and not observed at the level plotted in this figure; at a lower level this peak is observable in the position indicated by the box. Side-chain amide resonances of Asn and Gln residues are connected by horizontal lines.

gradient minimization. The experimental distance and dihedral restraints were applied using a square-well potential function with force constants of 25 kcal·mol^{-1}·Å^{-2} and 100 kcal·mol^{-1}·rad^{-2}, respectively. The structures were then equilibrated at 500 K for 1.5 ps, with the experimental restraint force constants scaled by a factor of 0.1. The experimental restraint force constants were increased to their full values (see above) during the next 2 ps. The system remained at 500 K for a further 1 ps before being cooled to 0 K over 3 ps. Following another 1 ps at 0 K the system was again minimized for 100 cycles of steepest descents and 2000 steps of conjugate gradient minimization. All calculations were performed on a Silicon Graphics Challenge XL computer.

RESULTS AND DISCUSSION

Resonance Assignments. Nearly complete backbone and side-chain ^1H assignments were obtained for the 63-residue HRG-α EGF-like domain using standard methods utilizing DQF-COSY, 2Q, TOCSY, NOESY, and TOCSY-relayed NOESY spectra (Wüthrich, 1986; Chazin & Wright, 1988). Amino acid spin systems were identified using DQF-COSY, 2Q, and TOCSY spectra. The 2Q spectra were used to identify chemical shift degeneracy for a number of side-chain protons. Following initial spin system identification, NOESY spectra were used to identify sequential "through-space" connectivities. The TOCSY-relayed NOESY spectrum was particularly useful in resolving ambiguities resulting from degenerate $^1H^\alpha$ resonances. Most ambiguities involving amide protons were resolved by comparative analysis of spectra acquired at two temperatures, 20 and 30 °C. However, the degree of spectral overlap in the $^1H^N$ and $^1H^\alpha$ regions of the 2D homonuclear NOESY spectra hindered the assignment of structurally important NOE cross peaks, despite the fact that almost complete assignment of resonances was achieved by the homonuclear methods outlined above. We therefore produced a ^{15}N-labeled sample in order to improve resolution by taking advantage of the greater ^{15}N chemical shift dispersion in 3D ^{15}N-edited TOCSY and NOESY spectra. Three-dimensional ^{15}N-edited TOCSY and NOESY spectra acquired at 20 °C were analyzed to obtain ^{15}N chemical shifts and to confirm the previous ^1H resonance assignments. Figure 1 shows the 2D $^1H-^{15}N$ HSQC spectrum of the HRG-α EGF-like domain at 20 °C with the assignments indicated. The quality of the 3D $^1H-^{15}N$ NOESY data obtained for the ^{15}N-labeled sample is indicated in Figure 2, which shows strips taken parallel to the $F_1(^1H)$ axis for different $F_2(^{15}N)$ planes corresponding to residues 7−25, ordered according to their sequential assignments. Stereospecific assignments for the β-methylene protons of the proline residues and the methyl group protons of two valine residues (Val15 and Val23) were obtained as described previously (Zuiderweg et al., 1985; Kline et al., 1989).

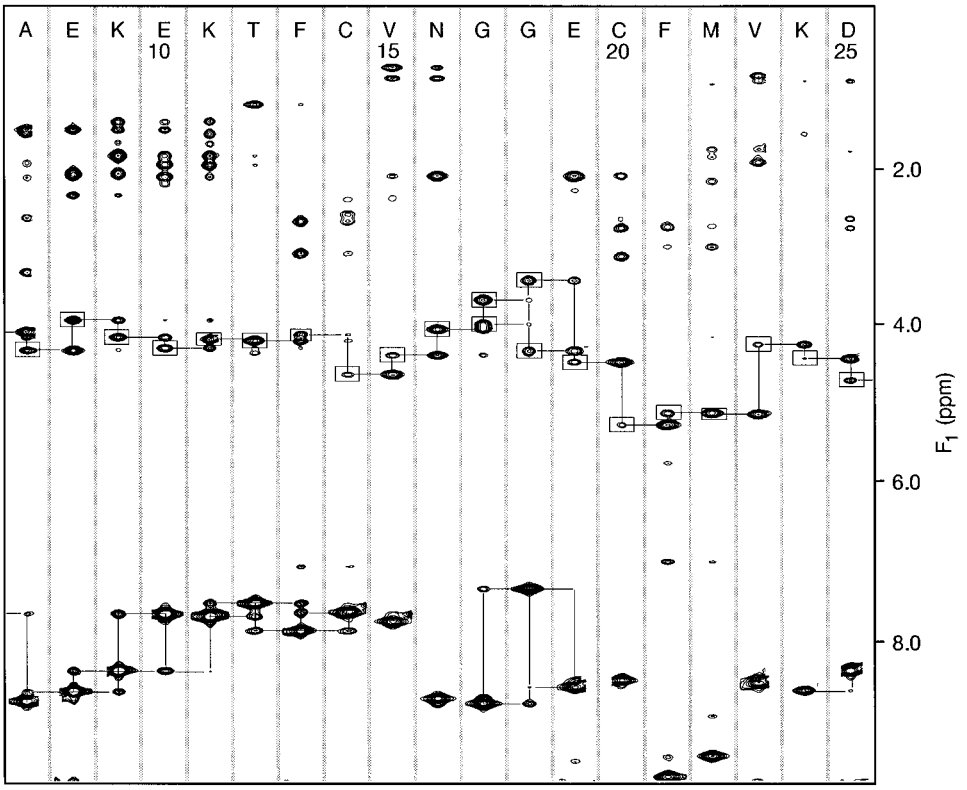

FIGURE 2: Strip plot corresponding to selected regions of amide planes for residues 7−25 taken from a 100 ms mixing time 3D $^{1}H-^{15}N$ NOESY-HSQC spectrum of the ^{15}N-labeled HRG-α EGF-like domain. The strips are arranged in sequential order, with the sequential assignment indicated at the top. Intraresidue $^{1}H^{N}-^{1}H^{\alpha}$ cross peaks, identified from a 3D $^{1}H-^{15}N$ TOCSY-HSQC spectrum, are boxed. Sequential $d_{NN}(i,i+1)$ and $d_{\alpha N}(i,i+1)$ NOEs are indicated by lines to the diagonal and intraresidue $^{1}H^{N}-^{1}H^{\alpha}$ cross peaks, respectively.

Stereospecific assignments for 13 of the remaining 36 β-methylenes having nondegenerate proton resonances were achieved as described in Materials and Methods. In addition, the α-protons of Gly18 and Gly42 were assigned stereospecifically on the basis of preliminary structure calculations. The ^{15}N and ^{1}H resonance assignments, with stereospecific assignments indicated where applicable, are listed in the supporting information, Table S1. A summary of the sequential NOE data obtained from the 2D NOESY and 3D NOESY-HSQC spectra is given in Figure 3.

A number of minor cross peaks are observed in the $^{1}H-^{15}N$ HSQC (Figure 1) and other spectra. These are due to the presence of two minor species comprising approximately 18% and 7% of the total sample (as judged by cross-peak intensities). LC-MS analysis of the NMR samples showed that about 20% of the protein has a mass 16 units higher than predicted for HRG-α and that this higher mass form elutes slightly later from the LC column (data not shown). Many of the minor-form spin systems have been sequentially assigned; most of the residues with shifted resonances in the minor forms are proximal to Met22 in the folded protein (see below). Distinct minor-form spin systems have also been assigned to residues 53 and 54, which are near to the only other methionine (Met51) in the protein. The only residues that show more than one distinct minor form are residues Val4 (aligned opposite Met22 in the major β-sheet; see later) and Val53. Together, these data suggest that the minor resonances result from oxidation of the methionine residues, Met22 or Met51. The two minor resonances observed for Val4 and Val53 may result from diastereomeric sulfoxides at the proximal methionine. Interestingly, methionine oxidation leads to loss of biological activity (M. X. Sliwkowski, unpublished observations). Attempts to separate the native and oxidized forms on a preparative scale have been unsuccessful.

Disulfide Bonds. In other EGF-like domains, the disulfide-bonding pattern has been shown to be 1−3, 2−4, 5−6. In order to verify that this was the disulfide arrangement of our recombinant HRG-α EGF-like domain (*i.e.*, Cys6−Cys20, Cys14−Cys34, Cys36−Cys45), we performed peptide mapping on the sample that was used for NMR spectroscopy. The protein was digested with trypsin, and the resulting peptides were analyzed by electrospray mass spectrometry. As shown in Table 1 only two disulfide-containing peptides were obtained: T2 + T4 + T6 and T7 + T8. Mass spectrometric analysis revealed that T7 + T8 was the expected tryptic peptide that contained Cys36 disulfide bonded to Cys45. To delineate the structure of the remaining two disulfides, the T2 + T4 + T6 peptide was further digested with *Staphylococcus aureus* V8 protease, and the resulting peptides were then isolated by reversed-phase HPLC. As shown in Table 1, analysis of the resulting V8 peptide digest resulted in the expected assignment of the remaining disulfide bonds *i.e.*, Cys6−Cys20 and Cys14−Cys34. The disulfide bonds thus determined were applied as covalent restraints in both the DG and rMD structure calculations.

Structure Determination. A total of 794 nonredundant NOE distance restraints were derived from analysis of NOESY spectra as described in Materials and Methods; these include 148 non-redundant intraresidue, 209 sequential, 153 medium-range ($1 < |i-j| < 5$), and 284 long-range ($|i-j| \geq 5$) restraints. The distribution of interresidue NOE distance restraints as a function of amino acid sequence is plotted in Figure 4A. Torsion angle restraints were obtained for 22 ϕ angles and 23 χ_1 angles as described in Materials

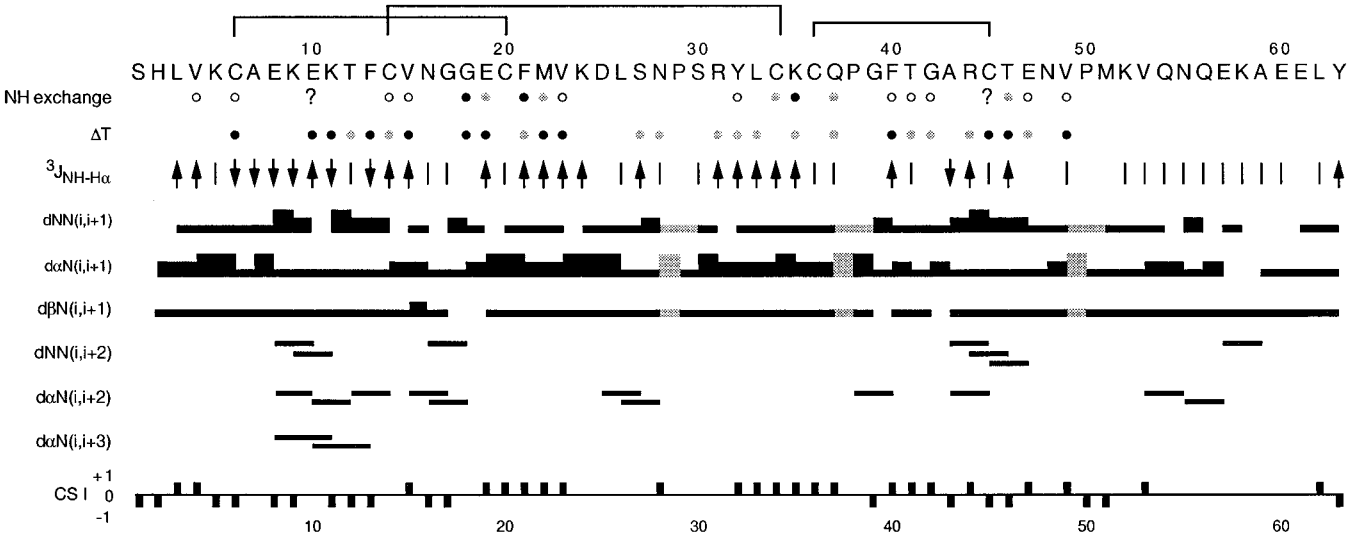

FIGURE 3: Summary of the sequential NOE connectivities, amide proton exchange and resonance temperature dependence, coupling constant, and $^1H^\alpha$ chemical shift data for the HRG-α EGF-like domain. The sequence numbering shown and used throughout this work (1−63) corresponds to residues 177−239 of HRG-α. Sequential NOE connectivities involving the $^1H^\delta$ of proline residues are denoted by shaded bars; all other sequential connectivities are indicated by filled bars. The relative intensities of the sequential NOEs are indicated by the thickness of the bars between adjacent residues. Measurable backbone amide proton exchange rates are catagorized according to calculated protection factors as follows (NH exchange): filled circles, >450; shaded circles, 200−450; open circles, <200. Cross peaks for Glu10 and Cys45 are degenerate in the TOCSY spectra used to determine the amide proton/deuterium exchange rates; one or both of these amide protons is significantly protected from exchange. Backbone amide proton chemical shift dependence (ΔT) was estimated from assignments obtained at two temperatures, 20 and 30 °C: resonances that shift by <4 ppb/°C are indicated by shaded circles; those that shift by <2 ppb/°C are indicated by filled circles. Measured $^3J_{H^N-H^\alpha}$ coupling constants are indicated as follows: ↓, J < 5 Hz; |, 5 Hz ≤ J ≤ 8 Hz; ↑, J > 8 Hz. The $^1H^\alpha$ chemical shift index (CSI) (Wishart et al., 1992) for each residue is plotted at the bottom of the figure.

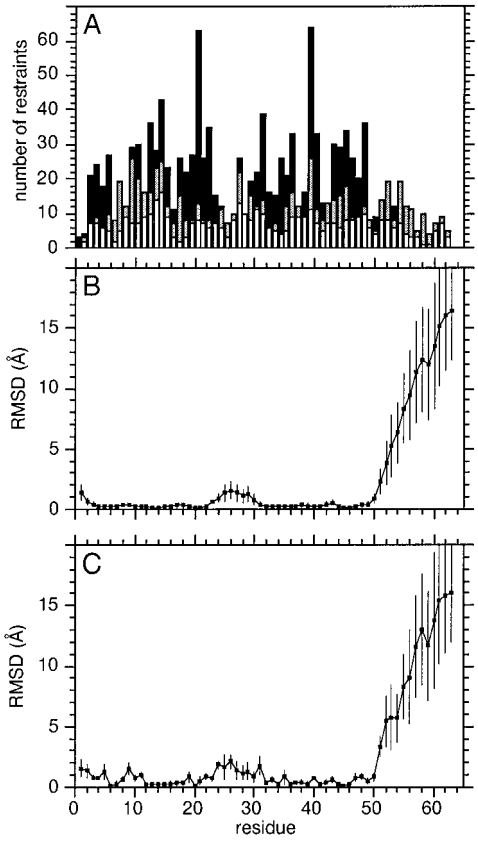

FIGURE 4: Residue-based summary of interresidue NOE distance restraints (A) and atomic rms distribution (mean ± SD) of the 20 final structures about the mean coordinates for backbone heavy atoms (B) and all heavy atoms (C). Sequential, medium-range ($1 < |i - j| < 5$), and long-range ($|i - j| \geq 5$) NOEs in (A) are indicated by open, shaded, and filled bars, respectively.

and Methods. A further 20 ϕ angle restraints were applied in cases where a negative ϕ angle could clearly be identified from NOESY data. In addition, 28 hydrogen bond distance restraints were applied for 14 hydrogen bonds identified on the basis of characteristic NOEs, reduced amide proton/deuterium exchange rates, reduced amide proton resonance temperature coefficients, and the results of preliminary structure calculations. The total number of experimentally derived restraints was thus 887, giving a total of 14.1 restraints per residue. Additional torsion angle restraints were applied to maintain the planarity of the peptide bonds ($\omega = 180 \pm 5°$) and the planarity of the side-chain amide groups of asparagine and glutamine residues ($\chi_{3,4} = 180 \pm 10°$). Observation of strong $^1H^\alpha$ to proline $^1H^\delta$ sequential NOEs, together with the absence of sequential $^1H^\alpha-^1H^\alpha$ NOEs, indicates that the three proline residues have trans peptide conformations; trans peptide restraints were therefore also applied to each proline residue. The additional torsion angle restraints were applied to supplement the force field only and were therefore not included in the above restraint count or subsequent analysis of restraint violations.

The 20 structures with the lowest residual restraint violation energies following the rMD calculations were selected to represent the solution structure of the HRG-α EGF-like domain. Structural statistics for these final 20 structures are summarized in Table 2. The overall residual restraint violation energies in these structures are low (3.4 ± 0.3 kcal·mol^{-1}); there are no interproton distance or torsion angle violations greater than 0.14 Å or 2.1°, respectively. The atomic rms deviations for backbone and heavy atoms, and angular order parameters (Hyberts et al., 1992) for ϕ and ψ torsion angles, are plotted as a function of residue number in Figures 4 and 5, respectively. Best fit superpositions of residues 1−50 of the final 20 structures on the mean coordinates are shown in Figure 6. Excluding residues 1−2, 24−30, and 50−63, which are clearly defined poorly by the data (Figures 4 and 5), the atomic rms differences for the final 20 structures with respect to the mean coordinate positions are 0.29 ± 0.07 Å for the backbone atoms and

Table 2: Structural Statistics

	final structures	minimized mean
rms deviation from exptl distance restraints (Å)		
NOE (794)	0.012 ± 0.001	0.011
H-bond (28)	0.011 ± 0.003	0.009
rms deviation from exptl dihedral restraints (deg)		
ϕ angles (42), χ_1 angles (23)	0.268 ± 0.054	0.198
NOE distance restraint violations		
no. >0.01 Å	53.2 ± 3.5	56
no. >0.1 Å	1.4 ± 0.9	0
maximum (Å)	0.12 ± 0.01	0.09
dihedral angle violations		
no. > 0.1°	7.2 ± 1.2	7
no. >1°	2.0 ± 1.1	1
maximum (deg)	1.4 ± 0.3	1.1
rms deviations from idealized covalent geometry[a]		
bonds (Å) (1000)	0.0047 ± 0.0001	0.0047
angles (deg) (1824)	1.51 ± 0.04	1.51
planes (deg) (189)	2.01 ± 0.11	2.18
energies (kcal·mol^{-1})		
$F_{\text{restraint}}$[b]	3.4 ± 0.3	3.0
F_{bond}	7.4 ± 0.4	7.3
F_{angle}	58.2 ± 3.2	58.5
F_{torsion}	60.5 ± 3.1	57.5
F_{plane}	1.4 ± 0.1	1.5
F_{vdW}[c]	−176.5 ± 6.0	−177.7
F_{elec}[d]	−138.1 ± 3.9	−139.1
F_{total}	−210.0 ± 10.9	−215.0
atomic rms differences (Å)[e]	backbone (N, C$^\alpha$, C)	all heavy atoms
final ensemble vs mean	0.29 ± 0.07	0.80 ± 0.11
final ensemble vs minimized mean	0.32 ± 0.09	0.99 ± 0.21
mean vs minimized mean	0.14	0.60

[a] Idealized covalent geometry is defined by the AMBER force field as implemented within DISCOVER. [b] The final values of the square-well NOE and dihedral angle potentials are calculated with force constants of 25 kcal·mol^{-1}·Å^{-2} and 100 kcal·mol^{-1}·rad^{-2}, respectively. [c] F_{vdW} is the Lennard-Jones van der Waals energy calculated with the all-atom AMBER force field and a 12 Å cutoff. [d] F_{elec} is calculated using a distance-dependent dielectric constant, $\epsilon = 4r$. [e] The atomic rms differences were calculated for residues 3−23 and 31−49 for the 20 final structures. The mean coordinates were obtained by averaging the coordinates of the 20 individual structures that were best fit to each other using the backbone atoms (N, C$^\alpha$, C) of residues 3−23 and 31−49. The minimized mean is the structure obtained by restrained minimization of the mean coordinates (due to the degree of disorder in the C-terminal region of the 20 final structures, residues 50−63 of the mean structure were replaced with the corresponding residues from the single structure that most resembles the mean prior to restrained minimization).

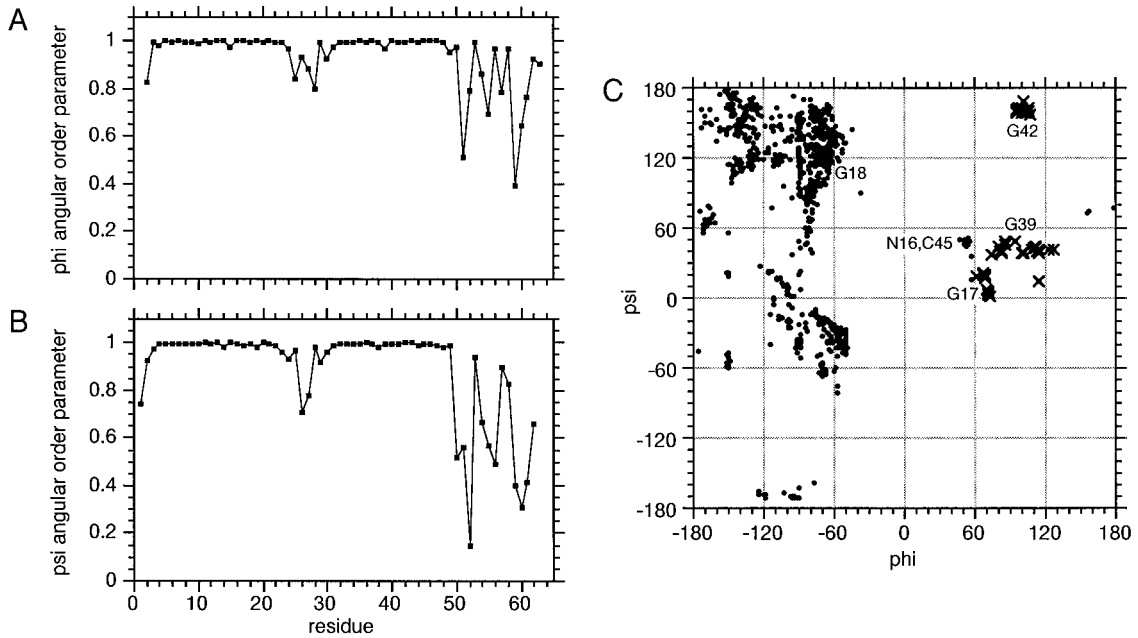

FIGURE 5: Angular order parameters for ϕ (A) and ψ (B) angles calculated from the 20 final structures and a Ramachandran ϕ,ψ plot (C) for residues 3−49 only of the 20 final structures. The four glycine residues, indicated by crosses, and Asn16 and Cys45 are labeled in (C).

0.80 ± 0.11 Å for all heavy atoms (Table 2). For residues 3−49, 79.0 ± 3.1% of the ϕ,ψ torsion angles lie within the most favored regions of a Ramachandran ϕ,ψ plot, 19.6 ± 3.2% lie within the additionally allowed regions, and 1.4 ± 1.8% lie in the generously allowed regions (Laskowski et al., 1993) (Figure 5C). Only three residues in the range 3−49 are found in the generously allowed region: Leu26 in one structure; Ser27 in three structures; and Ser30 in seven structures. Thus, all residues found in the generously allowed region of the Ramachandran ϕ,ψ plot are located in the

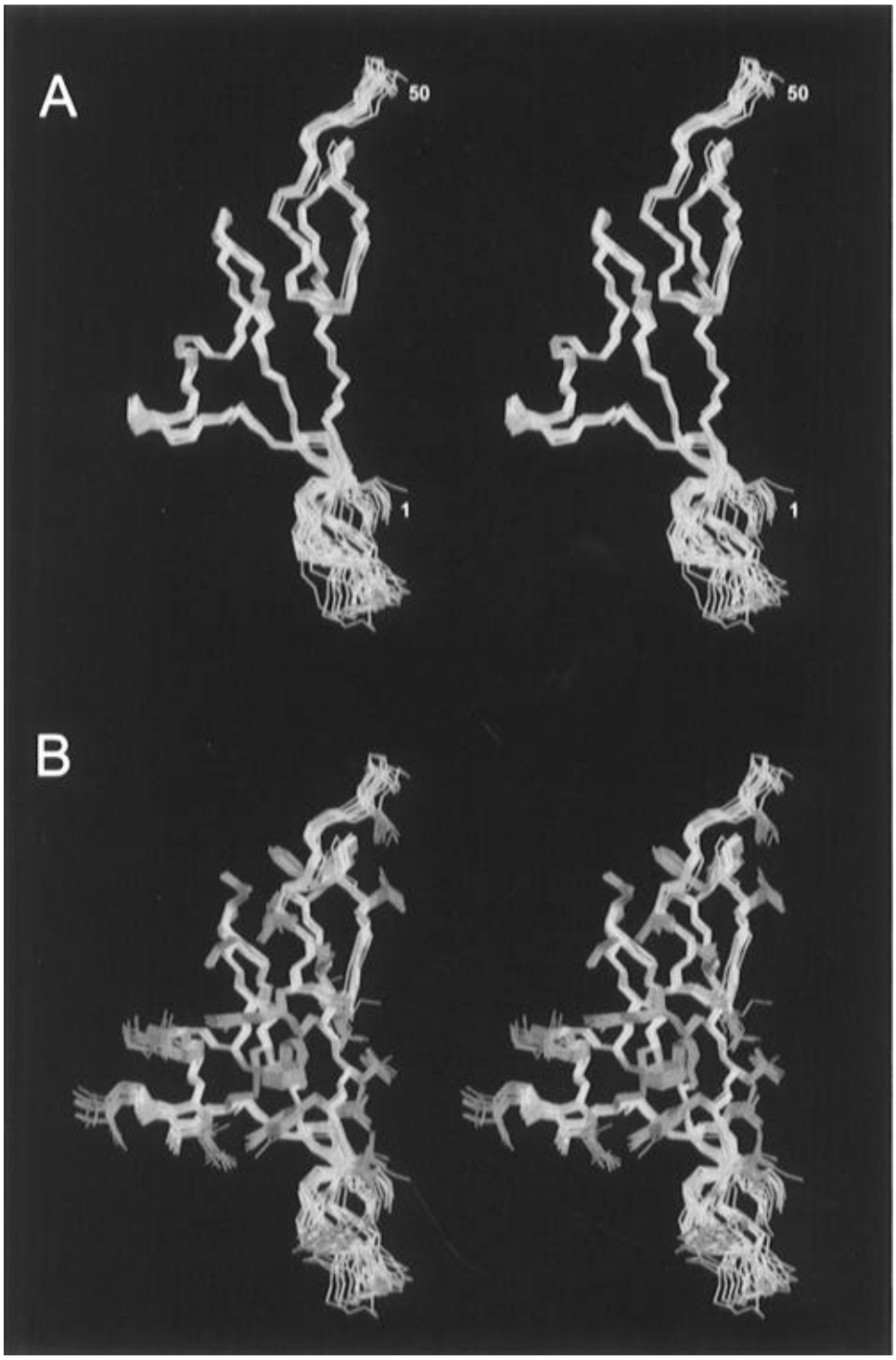

FIGURE 6: Stereoviews showing best fit superpositions of the backbone atoms from 19 of the 20 final structures (structure 3, which is "out of family" in the vicinity of Asn16, has been omitted for clarity). (A) The backbone atoms only of residues 1−50 are shown. The superpositions were optimized using residues 3−23 and 31−49. (B) The same superpositions as (A) but showing the side-chain heavy atoms of Ala7 and Ala43 and those residues having χ_1 angular order parameters ≥0.9 (Leu3, Cys6, Glu8, Glu10, Lys11, Thr12, Phe13, Cys14, Val15, Asn16, Cys20, Phe21, Val23, Pro29, Tyr32, Leu33, Cys34, Lys35, Cys36, Gln37, Pro38, Phe40, Thr41, Arg44, Cys45, Thr46, Val49). The figure was produced using the program MIDAS (Ferrin et al., 1988).

disordered region 24−30. Positive ϕ angles are observed for three glycine residues, Gly17, Gly39, and Gly42, and for Asn16 and Cys45. The two non-glycine residues were clearly identified as having positive ϕ angles as they both have $^3J_{H^N-H^\alpha}$ coupling constants of ∼7 Hz and intraresidue $^1H^\alpha-^1H^N$ NOEs that are stronger than the sequential $^1H^\alpha-^1H^N$ NOE from the preceding residue (Ludvigsen & Poulsen, 1992).

Description of Structure. The secondary and tertiary structure of the HRG-α EGF-like domain is represented schematically in Figure 7. A Kabsch and Sander (1983) type analysis of the 20 final structures, using the program PROCHECK (Laskowski et al., 1993), indicates a three-stranded β-sheet comprising residues Leu3−Lys5, Glu19−Val23, and Tyr32−Lys35 and a small two-stranded β-sheet comprising residues Phe40−Thr41 and Glu47−Asn48 (residues His2, Cys6, Lys24, Arg31, Gly39, and Val49 are additionally classified as being extensions of the β-strands). The secondary structure is consistent with that deduced from a qualitative analysis of the sequential NOE, $^1H^N$ exchange,

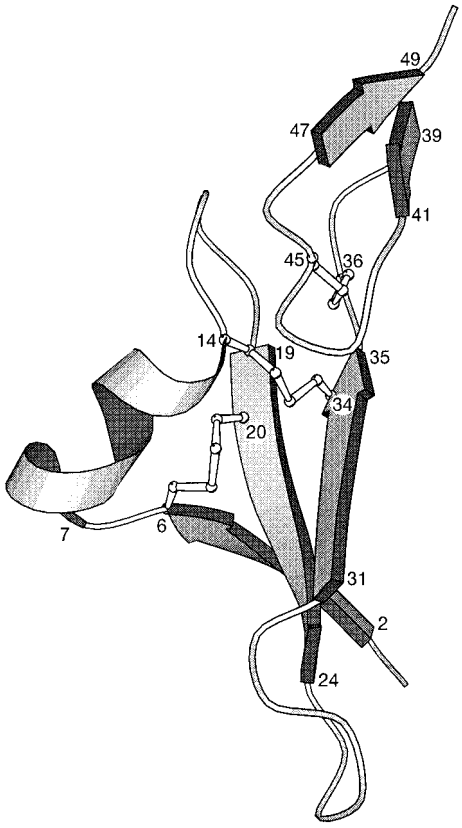

FIGURE 7: Schematic representation of the HRG−α EGF-like domain structure (residues 1−50), highlighting the elements of secondary structure and the disulfide bridges. The figure was produced using the program MOLSCRIPT (Kraulis, 1991).

Table 3: Observed Hydrogen Bonds

donor	acceptor	number[a]	distance (Å)[b]	angle (deg)[c]
Val4 H^N	Met22 O	20*	2.16 ± 0.07	161 ± 6
Cys6 H^N	Cys20 O	20*	2.05 ± 0.06	172 ± 5
Glu10 H^N	Ala7 O	20	1.99 ± 0.06	135 ± 7
Lys11 H^N	Ala7 O	19	1.97 ± 0.05	128 ± 4
Phe13 H^N	Glu10 O	20	1.96 ± 0.02	156 ± 2
Val15 H^N	Arg44 O	20*	2.14 ± 0.05	159 ± 5
Asn16 $H^{\delta 21}$	Cys45 O	19	1.91 ± 0.01	169 ± 3
Gly18 H^N	Val15 O	20*	2.04 ± 0.01	148 ± 7
Glu19 H^N	Lys35 O	20*	2.22 ± 0.04	152 ± 5
Phe21 H^N	Leu33 O	20*	2.10 ± 0.09	138 ± 3
Met22 H^N	Val4 O	20*	1.96 ± 0.05	146 ± 5
Val23 H^N	Arg31 O	20*	1.96 ± 0.09	168 ± 6
Lys24 H^N	His2 O	18	2.00 ± 0.16	154 ± 11
Ser27 H^N	Asp25 O	13	2.00 ± 0.04	144 ± 5
Asn28 $H^{\delta 22}$	Val23 O	15	2.08 ± 0.09	145 ± 10
Leu33 H^N	Phe21 O	20*	1.96 ± 0.03	169 ± 5
Lys35 H^N	Glu19 O	20*	1.94 ± 0.04	154 ± 3
Cys36 H^N	Cys34 O	19	2.32 ± 0.06	125 ± 3
Gln37 $H^{\epsilon 21}$	Gly17 O	17	1.94 ± 0.01	161 ± 6
Thr41 H^N	Glu47 O	20*	1.95 ± 0.04	150 ± 2
Gly42 H^N	Thr41 $O^{\gamma 1}$	13	2.20 ± 0.04	123 ± 2
Arg44 $H^{\eta 21}$	Thr12 O	20	1.93 ± 0.01	160 ± 2
Arg44 H^{ϵ}	Phe13 O	20	2.01 ± 0.04	148 ± 4
Cys45 H^N	Gly42 O	20*	2.02 ± 0.03	161 ± 5
Gly47 H^N	Thr41 O	20*	2.21 ± 0.06	145 ± 3
Val49 H^N	Gly39 O	20*	1.98 ± 0.09	163 ± 8
Gln54 H^N	Lys52 O	17	2.09 ± 0.14	143 ± 8

[a] The number of structures of the final 20 for which the listed hydrogen bond is observed. Asterisks (*) indicate those hydrogen bonds for which distance restraints were applied in the final structure calculations. [b] The distance is the mean proton−oxygen distance (±SD) in the structures for which a hydrogen bond is observed. [c] The angle is the mean N−H- - -O angle (±SD) in the structures for which a hydrogen bond is observed.

$^1H^N$ chemical shift temperature dependence, $^3J_{H^N-H^\alpha}$ coupling constant, and $^1H^\alpha$ chemical shift index (Wishart et al., 1992) data summarized in Figure 3, together with the observation of long-range backbone−backbone NOE connectivities [$d_{NN}(i,j)$, $d_{\alpha N}(i,j)$, and $d_{\alpha\alpha}(i,j)$] as indicated in supporting information, Figure S1. The relative orientation of the two β-sheet subdomains is well determined and is stabilized by four hydrogen-bonding interactions, Val15 H^N → Arg44 O, Asn16 $H^{\delta 21}$ → Cys45 O, Arg44 $H^{\eta 21}$ → Thr12 O, and Arg44 H^{ϵ} → Phe13 O (Table 3), as well as potentially favorable hydrophobic interactions between the side chains of Arg44 and those of Phe13 and Val15.

The C-terminal residues, Met51−Tyr63, are clearly disordered (Figures 4 and 5) and flexible (as judged from ^{15}N relaxation measurements; W. J. Fairbrother, unpublished results) in solution. A number of medium-range NOE cross peaks observed in this region (Figures 3 and 4A) probably result from transient loops and turns and lead to a more compact structure than would be expected for a completely unrestrained peptide segment. Interestingly, the more ordered region of the protein, residues 1−50, has been shown recently to be the minimal requirement for binding to cellular receptors and for stimulation of *Erb*B-2 phosphorylation (Barbacci et al., 1995). The 50-residue fragment was also shown to be ∼10-fold more potent than the 63-residue fragment studied here; however, further truncation of residues Val49 and Pro50 reduced both receptor binding and phosphorylation activity by >100-fold (Barbacci et al., 1995). Similar results were reported for HRG-β (Barbacci et al., 1995). The lower potency of the 63-residue protein relative to the 50-residue form suggests that the flexible C-terminal tail interferes with receptor binding, possibly through a steric effect.

In addition to the β-sheet secondary structure a number of hydrogen-bonded turn structures are identified that are consistent with observed medium-range NOEs (Figure 3). In 10 of the final 20 structures an α-helical turn is identified between residues Ala7 and Thr12, while in the remaining 10 structures a 3_{10}-helical turn is identified between residues Glu10 and Cys14; the conformation of this region is illustrated for the final 20 structures in Figure 8A. Hydrogen bonds are found between the amide protons of both Glu10 and Lys11 and the carbonyl oxygen of Ala7 and between the amide proton of Phe13 and the carbonyl oxygen of Glu10 (Table 3, Figure 8A). Each of these amide protons has a significantly reduced temperature coefficient (<2 ppb/°C), consistent with their observed participation in hydrogen bonds; however, none were identified as exchanging slowly with solvent (Glu10 is ambiguous in this regard) (Figure 3), suggesting that the observed hydrogen bonds are probably weaker than those identified in the regular β-sheet secondary structure. The helical loop region is "attached" to the major β-sheet via disulfide bridges at either end (Cys6−Cys20 and Cys14−Cys34). Residues Val15−Gly18 form a well-defined type I′ β-turn (Wilmot & Thornton, 1988) preceding strand II of the major β-sheet (Figure 8B). The hydrogen bond observed between Gly18 H^N and Val15 O (Table 3, Figure 8B) is consistent with the reduced amide proton/deuterium exchange rate and temperature coefficient found for Gly18 (Figure 3). The minor β-sheet strands IV and V are connected by a type I β-turn defined by residues Gly42−Cys45 (Figure 8C) with a β-bulge at residue Thr46. In this case a hydrogen bond is observed between Cys45 H^N and

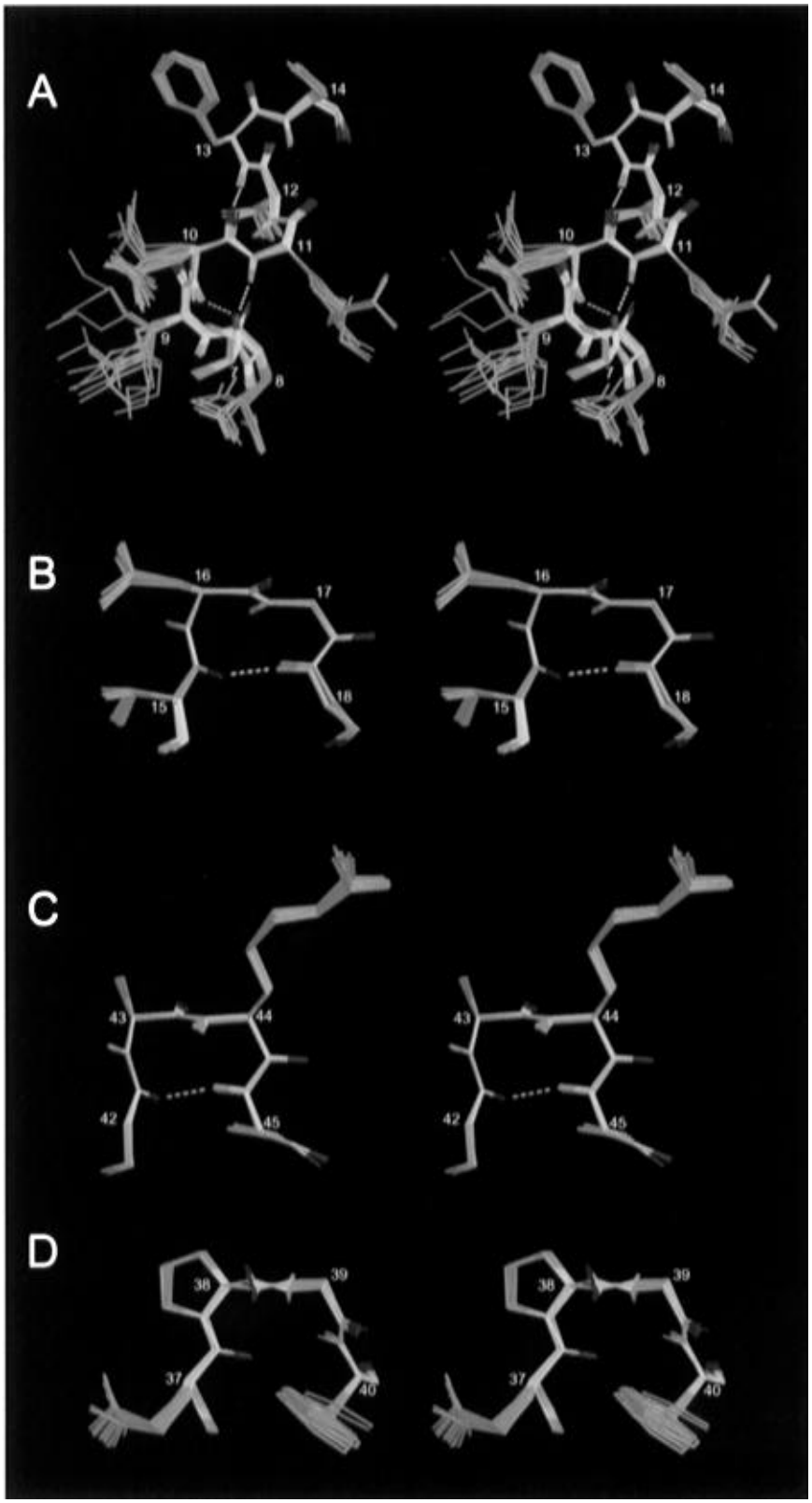

FIGURE 8: Stereoviews showing best fit superpositions of the backbone atoms (N, C, C^{α}, O) for selected turns: residues 7−14 (A), residues 15−18 (structure 3, which is "out of family" in the vicinity of Asn16, has been omitted for clarity) (B), residues 42−45 (C), and residues 37−40 (D). The backbone heavy atoms are shown in cyan, amide hydrogens in blue, carbonyl oxygens in red, and side-chain heavy atoms in pink. Hydrogen bonds are indicated by the dashed lines. The figure was produced using the program MIDAS (Ferrin et al., 1988).

Gly42 O (Table 3, Figure 8C). The hydrogen bond is supported by observation of a reduced temperature coefficient (<2 ppb/C°) for the amide proton of Cys45; unfortunately, the amide proton/deuterium exchange rate for Cys45 could not be determined due to resonance overlap with Glu10 (Figure 3). A bend identified at Pro38−Gly39, between β-strands III and IV, appears to be a distorted type II β-turn (Figure 8D). The hydrogen-bond expected between Phe40 H^N and Gln37 O for a type II β-turn is, however, not observed, even though the amide proton/deuterium exchange rate and temperature coefficient of Phe40 are both reduced (Figure 3). Additional hydrogen bonded turns are found in other regions in some of the final 20 structures, including the conformationally disordered Ω-loop Lys24−Ser30 and

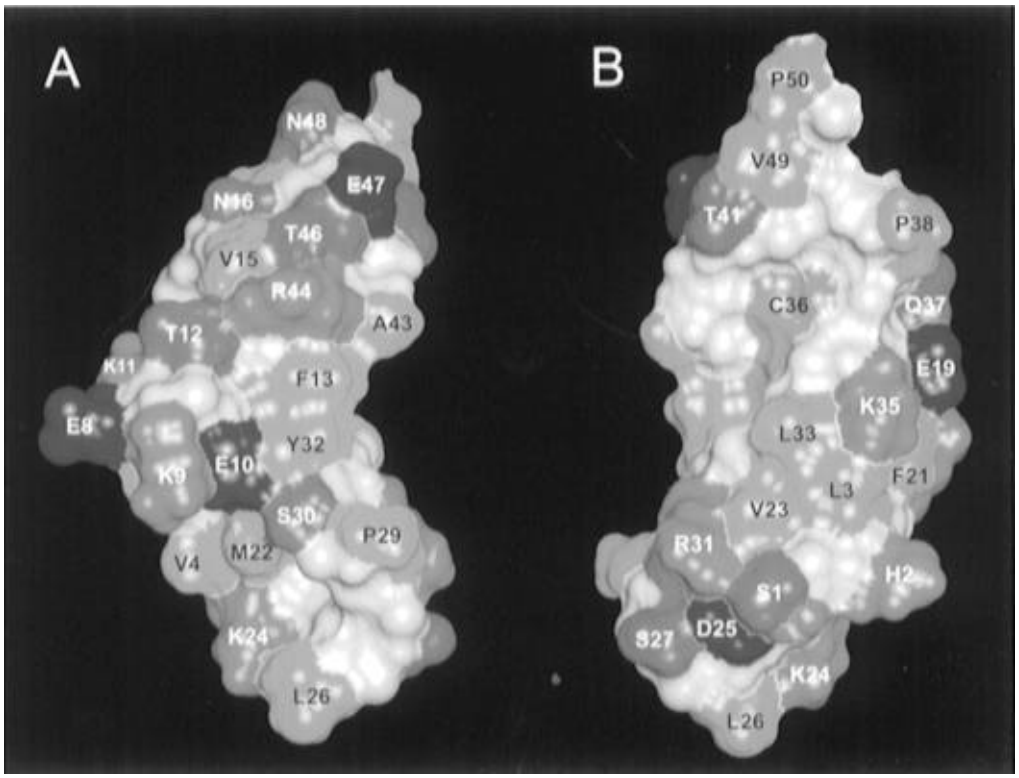

FIGURE 9: Two views (A and B) of the minimized mean structure showing the solvent-accessible surface for residues 1−50. Atoms are colored as follows: main chain (N, C, C^{α}, O, H^{N}, H^{α}), gray; hydrophobic side chains (Ala, Cys, Leu, Met, Phe, Pro, Tyr, Val), yellow; uncharged hydrophilic side chains (Asn, Gln, Ser, Thr), green; negatively charged side chains (Asp, Glu), red; positively charged side chains (Arg, His, Lys), blue; N-terminus, blue. The figure was produced using the program INSIGHT II (Biosym Technolgies, Inc., San Diego).

C-terminal region (50−63). A complete list of hydrogen bonds found in >50% of the final structures is given in Table 3.

The three disulfide bridges are well-defined; the Cys6−Cys20 disulfide bridge is left-handed, while the other two (Cys14−Cys34 and Cys36−Cys45) have right-handed conformations. In all cases the χ_1 dihedral angles are well-defined by the NOE and coupling constant data (χ_1 is approximately −60° for Cys6, Cys14, Cys34, Cys36, and Cys45 and 180° for Cys20). Due to unusual χ_2 values, none of the cystine conformations appear consistent with previously identified disulfide bridge conformational families (Katz and Kossiakoff, 1986; Srinivasan et al., 1990). However, the dihedral energies, calculated as described by Katz & Kossiakoff (1986), are low with values of ∼1.1, 2.0, and 0.7 kcal·mol^{-1} for disulfides Cys6−Cys20, Cys14−Cys34, and Cys36−Cys45, respectively, suggesting that the observed conformations are energetically reasonable. Interestingly, the conformation found for the disulfide bond between Cys6 and Cys20, which are also hydrogen-bonded to each other (Table 3), has previously been observed for a similarly hydrogen bonded cystine in a 2.0 Å resolution crystal structure of the snake venom zinc endopeptidase adamalysin II (Gomis-Rüth et al., 1994) (PDB accession code 1iag). Alternatively, the determined disulfide conformations may represent the averages of conformations that exchange in solution. Indeed, analysis of ^{15}N relaxation data reveals significant millisecond time-scale internal motions that may be consistent with disulfide conformational exchange (W. J. Fairbrother, unpublished results).

With the exception of the three disulfides, the HRG-α EGF-like domain lacks a hydrophobic core. Exposed hydrophobic residues are found, however, on either surface of the major β-sheet (Leu3, Phe21, Val23, and Leu33 on one side and Val4, Met22, and Tyr32, which also packs against Phe13, on the other side), as well as between the two subdomains (see above). The hydrophobic clusters can be seen clearly in Figure 9. The significant areas of exposed hydrophobic side chains may lead to nonspecific aggregation at the high concentrations required for structural analysis; concentration-dependent aggregation has been observed in solution for both the HRG-α and, to a greater extent, the HRG-β1 EGF-like domains (W. J. Fairbrother, unpublished results).

Comparison with Other EGF Structures. A solution structure of the HRG-α EGF-like domain has been determined previously using 2D homonuclear NMR spectroscopy at pH 6.0, 37 °C (Nagata et al., 1994). Figure 10A compares the minimized mean structure, as described herein at pH 4.5, 20 °C, with the previously determined structure (Nagata et al., 1994). While the secondary structure and global fold of these two structures are similar, the overall rms deviation for the C^{α} atoms of the ordered residues Leu3−Val23 and Arg31−Val49 is relatively high at 2.43 Å (Figure 10). This may represent a real difference between the structures at pH 4.5 and pH 6.0 or alternatively may suggest that one or the other structure is less accurately defined. Comparison of 2D TOCSY and NOESY spectra of unlabeled protein acquired at the two pH values indicates, however, that no significant structural differences exist between the proteins under these different sample conditions.[1] The use of ^{15}N-labeled recombinant protein at pH 4.5 for the present study has resulted in the determination of ∼50% more NOE-derived distance restraints (794 compared to 534) relative to the previously published structure determination at pH

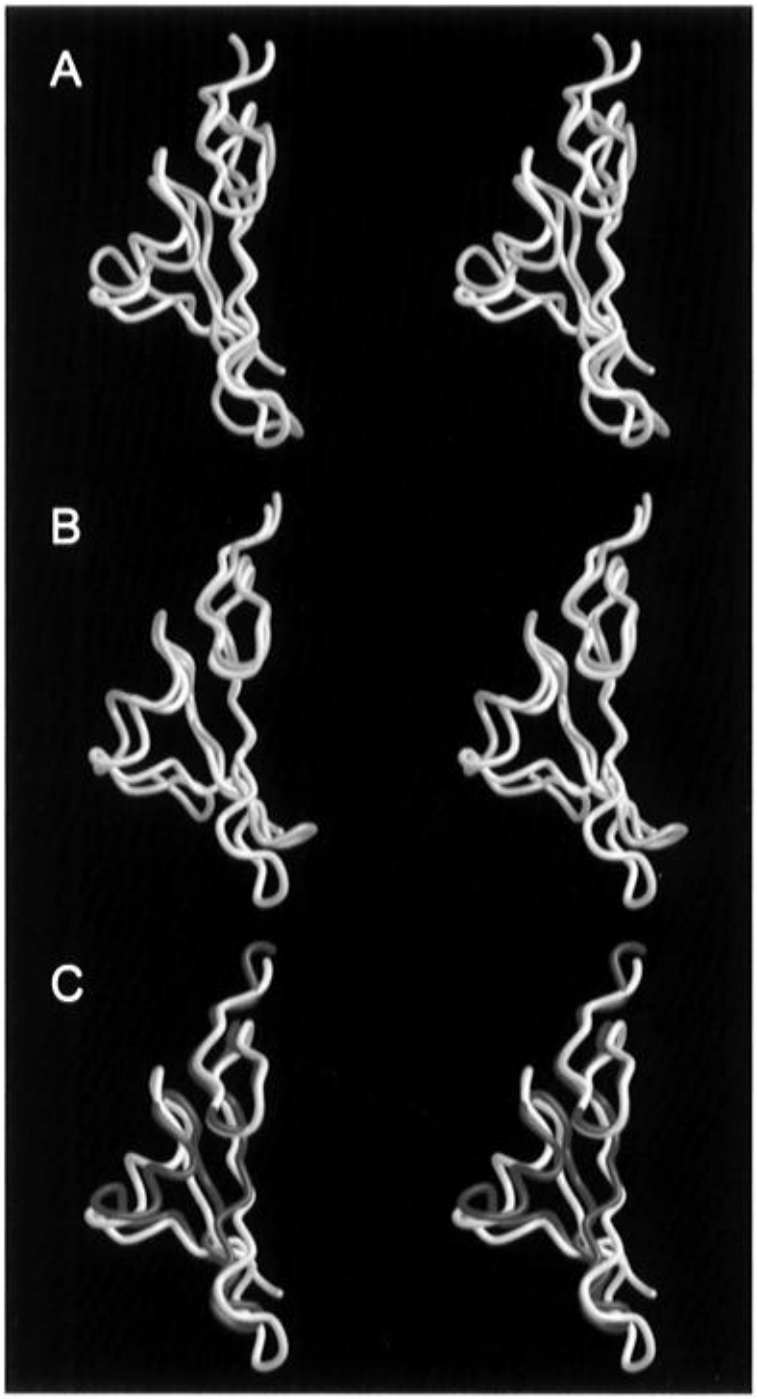

D

```
                1         10        20        30        40        50        60
HRGα      SHLVKCAEKEKTFCVNGGECFMVKDLSNPSRYLCKCQPGFTGARCTENVPMKVQNQEKAEELY

hEGF      NSDSECPLSHDGYCLHDGVCMYIEAL---DKYACNCVVGYIGERCQYRDLKWWEL

hTGF-α    VVSHFNDCPDSHTQFCFH-GTCRFLVQE---DKPACVCHSGYVGARCEHADLLA
```

FIGURE 10: Stereoviews showing tube representations of the best fit superpositions of C^{α} atoms of the minimized mean HRG-α EGF-like domain coordinates (blue) on the minimized mean structures of the HRG-α EGF-like domain determined at pH 6.0 (A, pink) (Nagata et al., 1994; PDB accession code 1HRE), human EGF (B, yellow) (Hommel et al., 1992; coordinates obtained via the IDC home page, http://nmra.ocms.ox.ac.uk), and human TGF-α (C, magenta) (Harvey et al., 1991; PDB accession code 2TGF) and the aligned amino acid sequences of these proteins (D). The residues shown in (A)−(C) correspond to the HRG-α EGF-like domain residues 1−50. The superpositions were optimized using residues 3−23 and 31−49 (A), 4−23 and 31−49 (B), and 4−15, 19−23, and 31−49 (C) [sequence numbering as in (D)]. Residues that are identical between the HRG-α EGF-like domain and either hEGF or hTGF-α are indicated in red in (D). The figure was produced using the program MIDAS (Ferrin et al., 1988).

6.0 (Nagata et al., 1994), together with increased numbers of dihedral angle restraints (42 ϕ and 23 χ_1 compared to 15 ϕ and 7 χ_1, respectively) and identification of a number of hydrogen bond restraints that are supported by reduced amide

proton exchange rates not observed at the higher pH. Increased numbers of restraints have previously been correlated with improvements in both precision and accuracy (Clore et al., 1993; Zhao & Jardetzky, 1994). Furthermore, comparison of the final restraint violation energies from the two different structure determinations reveals that the agreement between the final structures and the NMR-derived restraints used to calculate them is significantly better for the pH 4.5 structure ($F_{restraint} = 3.4 \pm 0.3$ kcal·mol^{-1}; Table 2) than that determined at pH 6.0 ($F_{restraint} = 187.2 \pm 8.5$ kcal·mol^{-1}; Nagata et al., 1994). Note, however, that such a comparison must be treated qualitatively because the two structures were calculated using different numbers of restraints (see above) and restraint force constants [for the present structure the restraint energies include contributions from square-well NOE and dihedral potentials with force constants of 25 kcal·mol^{-1}·Å^{-2} and 100 kcal·mol^{-1}·rad^{-2}, respectively, while the restraint energies for the structures of Nagata et al. (1994) are calculated using a square-well NOE potential with a force constant of 50 kcal·mol^{-1}·Å^{-2}]. Nevertheless, restraint energies of ~187 kcal·mol^{-1}·Å^{-2} for the previously published structure result from several violations >0.5 Å (Nagata et al., 1994) and indicate the existence of a number of other significant distance restraint violations >0.1 Å.

Structures have also been obtained previously for both EGF and TGF-α under a variety of solution conditions (Kline et al., 1990; Harvey et al., 1991; Hommel et al., 1992; Kohda & Inagaki, 1992a,b; Montelione et al., 1992; Moy et al., 1993). Parts B and C of Figure 10 show best fit superpositions (using the C$^{\alpha}$ atoms) of the minimized mean coordinates of human EGF (Hommel et al., 1992) and human TGF-α (Harvey et al., 1991), respectively, on the minimized mean coordinates of the HRG-α EGF-like domain, and Figure 10D shows the alignment of the primary sequences of these proteins. The atomic rms differences between the hEGF and hTGF-α structures and the HRG-α EGF-like domain are significantly lower than for the alignment between the two HRG-α EGF-like domain structures discussed above (Figure 10); the best fit C$^{\alpha}$ alignment of the HRG-α EGF-like domain residues Val4−Val23 and Arg31−Val49 with the corresponding residues of hEGF (Hommel et al., 1992), Ser4−Ile23 and Lys28−Asp46, has an rms difference of 1.39 Å; a similar C$^{\alpha}$ alignment of the HRG-α EGF-like domain residues Val4−Val15, Glu19−Val23, and Arg31−Val49 with the corresponding residues of hTGF-α (Harvey et al., 1991), Asn6−Phe17, Thr20−Leu24, and Lys29−Asp46, has an rms difference of 1.68 Å. Similar alignments with other reported EGF and TGF-α structures (Kline et al., 1990; Kohda & Inagaki, 1992b; Montelione et al., 1992; Moy et al., 1993) yield higher rms differences.

The HRG-α EGF-like domain has a three-residue insertion between β-strands II and III relative to the sequences of both hEGF and hTGF-α (Figure 10D). As a consequence the most significant structural difference between these proteins occurs in this loop region. The conformation of the adjacent N-terminal region preceding the first cysteine is also significantly different in the HRG-α EGF-like domain. In the reported EGF and TGF-α structures the N-terminal residues are disordered or form a poorly defined β-strand (Kline et al., 1990; Harvey et al., 1991; Hommel et al., 1992; Kohda & Inagaki, 1992b; Montelione et al., 1992; Moy et al., 1993), whereas in the HRG-α EGF-like domain structure this region forms a well-defined β-strand (strand I), which has both hydrogen-bonding (Table 3) and hydrophobic interactions with β-strand II (Figure 9); similar observations were made by Nagata et al. (1994). The N-terminal region of the HRG EGF-like domain has been implicated recently as being important for heregulin receptor binding (Barbacci et al., 1995). By substituting the five N-terminal residues of hEGF (NSDSE) with the corresponding residues from the HRG EGF-like domain (SHLVK), these workers produced a bifunctional agonist that binds with high affinity to both the heregulin and EGF receptors. Interestingly, the side chain of Val4 in β-strand I packs against Met22; oxidation of this methionine side chain inactivates heregulin. The above results, together with the finding that substitution of residues 21−33 in the HRG-β EGF-like domain with residues 21−30 of hEGF has no effect on heregulin receptor binding or *Erb*B-2 phosphorylation (Barbacci et al., 1995), suggest that the functional significance of the three-residue insertion between β-strands II and III in the HRG-α EGF-like domain (Figure 10D) is minimal.

Significant differences are also seen between the helical turn regions of the HRG-α EGF-like domain (Ala7−Phe13) and the hEGF/hTGF-α minimized mean structures (Figure 10B,C). The differences are less pronounced than those reported by Nagata et al. (1994), with the angle between the helical region and the major β-sheet being similar in each structure. The helical turn regions of hEGF and hTGF-α are less well defined than that of the HRG-α EGF-like domain, so the significance of the observed differences between these regions of the minimized mean structures is difficult to evaluate. However, as pointed out by Nagata et al. (1994), there is no sequence homology between the helical turn regions of HRG-α and hEGF/hTGF-α (Figure 10D); the charged residues Glu8-Lys9-Glu10-Lys11 in the helical turn region of the HRG-α EGF-like domain, together with Lys5, Glu19, and Lys35, form a "stripe" of charged residues on one face of the molecule. None of these charged residues are conserved in hEGF (Figure 10D); therefore, the fact that the hEGF/HRG-α N-terminal swap mutant discussed above binds to and activates the heregulin receptor (Barbacci et al., 1995) suggests that these charged residues, with the possible exception of Lys5, are not important for heregulin binding.

Excluding the N-terminal region (Ser1−Phe13), the disordered Ω-loop (Lys24−Ser30), and the disordered C-terminal region (Pro50−Tyr63), the C$^{\alpha}$ alignment between the HRG-α EGF-like domain and hEGF minimized mean structures is very good, with an rms difference of 0.98 Å [this is likely within the accuracy limits of both structures (Zhao & Jardetzky, 1994)]. In particular, the orientation of the minor β-sheet with respect to the major β-sheet is identical due to a similar set of interdomain interactions. These include interdomain hydrogen bonds involving Val15 H^{N} and the side chains of Asn16 and Arg44 (Table 3). The conserved Arg44 residue (Arg41 in hEGF) appears to be particularly important in stabilizing the structures of both

[1] The intensities of cross peaks to the amide proton of Gly42 are reduced in both the TOCSY and NOESY spectra at pH 6.0 relative to pH 4.5; this probably represents increased solvent exchange for this amide proton rather than a true structural difference. Only a few small chemical shift changes (<0.2 ppm) are observed and are restricted to solvent-exposed amide protons. These chemical shift differences also probably represent solvent-exchange effects rather than structural differences because the NOE patterns of these resonances remain unchanged.

the HRG-α EGF-like domain and hEGF (Hommel et al., 1992) as it contributes two hydrogen bonds (Table 3) in addition to hydrophobic interactions with the side chains of Phe13 (Tyr13 in hEGF) and Val15 (Leu15 in hEGF) (Figure 9). This residue has been shown to be absolutely required for EGF binding to its receptor (Engler et al., 1990; Hommel et al., 1991). Substitution of this residue with histidine disturbs the interface between the two subdomains of the hEGF structure such that a $^1H^\alpha-^1H^\alpha$ NOE observed between residues Cys14 and Arg41 in native hEGF is not observed in the mutant protein; gross structural changes were deemed not to have occurred, however (Hommel et al., 1991).

Leu47 of hEGF has also been found to be required for binding of hEGF to its receptor. The equivalent residue is Pro50 or Met50 in the HRG-α and HRG-β EGF-like domains, respectively. C-Terminal truncation prior to Pro50 in HRG-α or Met50 in HRG-β has been shown to reduce both the receptor binding and phosphorylation by >100-fold (Barbacci et al., 1995), suggesting that these residues are also important for binding of heregulin to its receptors. However, the fact that a leucine in this position also gives an active molecule in the bispecific hEGF N-terminal swap variant discussed above (Barbacci et al., 1995) suggests that the exact residue type is not critical, although a hydrophobic side chain may be required.

The mutagenesis data of Barbacci et al. (1995) suggest that both the N-terminal and C-terminal regions of the structured portion (residues Ser1−Pro50) of the HRG-α EGF-like domain are important for heregulin receptor binding and activity and that the N-terminal region is responsible for heregulin receptor specificity. These two regions are remote from each other in the folded protein, indicating that there are at least two receptor binding sites. The intervening residues, in particular those that are conserved between HRG-α and hEGF/hTGF-α (Figure 10D), may play purely structural roles by maintaining the appropriate distance and orientation between these two regions. The high-resolution solution structure of the HRG-α EGF-like domain presented here will aid in the design of more detailed mutagenesis experiments to test the functional importance of residues in these, and other, regions of the protein. In addition, understanding of the relationship between structure and function for this and related EGF-like domains will benefit from analysis of the internal dynamics of the protein. This is currently in progress using ^{15}N relaxation measurements and will be the subject of a future publication.

ACKNOWLEDGMENT

We thank James Bourell, Beth Gillece-Castro, and Kathy O'Connell for mass spectrometry analysis and Daniel Yansura for the original construction of the HRG-α EGF-like domain plasmid.

SUPPORTING INFORMATION AVAILABLE

One table listing ^{15}N and ^1H chemical shift assignments and one figure showing a schematic representation of the β-sheet secondary structure and the observed interstrand backbone−backbone NOE connectivities (4 pages). Ordering information is given on any current masthead page.

REFERENCES

Alamandi, M., Romano, A., Curia, M. C., Muraro, R., Fedi, P., Aaronson, S. A., Di Fiore, P. P., & Kraus, M. H. (1995) *Oncogene 10*, 1813−1821.

Altiok, N., Bessereau, J.-L., & Changeux, J.-L. (1995) *EMBO J. 14*, 4258−4266.

Archer, S. J., Ikura, M., Torchia, D. A., & Bax, A. (1991) *J. Magn. Reson. 95*, 636−641.

Barbacci, E. G., Guarino, B. C., Stroh, J. C., Singleton, D. H., Rosnack, K. J., Moyer, J. D., & Andrews, G. C. (1995) *J. Biol. Chem. 270*, 9585−9589.

Baselga, J., & Mendelsohn, J. (1994) *Pharmacol. Ther. 64*, 127−154.

Bax, A., & Davis, D. G. (1985) *J. Magn. Reson. 65*, 355−360.

Bodenhausen, G., Kogler, H., & Ernst, R. R. (1984) *J. Magn. Reson. 58*, 370−388.

Braunschweiler, L., & Ernst, R. R. (1983) *J. Magn. Reson. 53*, 521−528.

Braunschweiler, L., Bodenhausen, G., & Ernst, R. R. (1984) *Mol. Phys. 48*, 535−560.

Brünger, A. T., Clore, G. M., Gronenborn, A. M., & Karplus, M. (1986) *Proc. Natl. Acad. Sci. U.S.A. 83*, 3801−3805.

Carraway, K. L., III, & Cantley, L. C. (1994) *Cell 78*, 5−8.

Cavanagh, J., & Rance, M. (1992) *J. Magn. Reson. 96*, 670−678.

Chazin, W. J., & Wright, P. E. (1988) *J. Mol. Biol. 202*, 623−636.

Chu, G. C., Moscoso, L. M., Sliwkowski, M. X., & Merlie, J. P. (1995) *Neuron 14*, 329−339.

Clore, G. M., Brünger, A. T., Karplus, M., & Gronenborn, A. M. (1986) *J. Mol. Biol. 191*, 523−551.

Clore, G. M., Bax, A., & Gronenborn, A. M. (1991) *J. Biomol. NMR 1*, 13−22.

Clore, G. M., Robien, M. A., & Gronenborn, A. M. (1993) *J. Mol. Biol. 231*, 82−102.

Clubb, R. T., Ferguson, S. B., Walsh, C. T., & Wagner, G. (1994) *Biochemistry 33*, 2761−2772.

Davis, D. G. (1989) *J. Magn. Reson. 81*, 603−607.

Driscoll, P. C., Clore, G. M., Marion, D., Wingfield, P. T., & Gronenborn, A. M. (1990) *Biochemistry 29*, 3542−3556.

Earp, H. S., Dawson, T. L., Li, X., & Yu, H. (1995) *Breast Cancer Res. Treat. 35*, 115−132.

Englander, J. J., Calhoun, D. B., & Englander, S. W. (1979) *Anal. Biochem. 92*, 517−524.

Engler, D. A., Montelione, G. T., & Niyogi, S. K. (1990) *FEBS Lett. 271*, 47−50.

Falls, D. L., Rosen, K. M., Corfas, G., Lane, W. S., & Fischbach, G. D. (1993) *Cell 72*, 801−815.

Ferrin, T. E., Huang, C. C., Jarvis, L. E., & Langridge, R. (1988) *J. Mol. Graphics 6*, 13−27.

Fesik, S. W., & Zuiderweg, E. R. P. (1990) *Q. Rev. Biophys. 23*, 97−131.

Gomis-Rüth, F. X., Kress, L. F., Kellermann, J., Mayr, I., Lee, X., Huber, R., & Bode, W. (1994) *J. Mol. Biol. 239*, 513−544.

Graus-Porta, D., Beerli, R. R., & Hynes, N. E. (1995) *Mol. Cell. Biol. 15*, 1182−1191.

Groenen, L. C., Nice, E. C., & Burgess, A. W. (1994) *Growth Factors 11*, 235−257.

Guy, P. M., Platko, J. V., Cantley, L. C., Cerione, R. A., & Carraway, K. L., III (1994) *Proc. Natl. Acad. Sci. U.S.A. 91*, 8132−8136.

Harvey, T. S., Wilkinson, A. J., Tappin, M. J., Cooke, R. M., & Campbell, I. D. (1991) *Eur. J. Biochem. 198*, 555−562.

Havel, T. F. (1991) *Prog. Biophys. Mol. Biol. 56*, 43−78.

Ho, W.-H., Armanini, M. P., Nuijens, A., Phillips, H. S., & Osheroff, P. L. (1995) *J. Biol. Chem. 270*, 14523−14532.

Holmes, W. E., Sliwkowski, M. X., Akita, R. W., Henzel, W. J., Lee, J., Park, J. W., Yansura, D., Abadi, N., Raab, H., Lewis, G. D., Shepard, H. M., Kuang, W.-J., Wood, W. I., Goeddel, D. V., & Vandlen, R. L. (1992) *Science 256*, 1205−1210.

Hommel, U., Dudgeon, T. J., Fallon, A., Edwards, R. M., & Campbell, I. D. (1991) *Biochemistry 30*, 8891−8898.

Hommel, U., Harvey, T. S., Driscoll, P. C., & Campbell, I. D. (1992) *J. Mol. Biol. 227*, 271−282.

Hyberts, S., Goldberg, M. S., Havel, T. F., & Wagner, G. (1992) *Protein Sci. 1*, 736−751.

Hynes, N. E. (1993) *Semin. Cancer Biol. 4*, 19−26.

Hynes, N. E., & Stern, D. F. (1994) *Biochim. Biophys. Acta 1198*, 165−184.

Kabsch, W., & Sander, C. (1983) *Biopolymers 22*, 2577−2637.

Katz, B. A., & Kossiakoff, A. (1986) *J. Biol. Chem. 261*, 15480−15485.

Kessler, H., Gemmecker, G., & Steuernagel, S. (1988) *Angew. Chem., Int. Ed. Engl. 27*, 564−566.
Kim, H. H., Sierke, S. L., & Koland, J. G. (1994) *J. Biol. Chem. 269*, 24747−24755.
Kline, A. D., Braun, W., & Wüthrich, K. (1989) *J. Mol. Biol. 104*, 675−724.
Kline, T. P., Brown, F. K., Brown, S. C., Jeffs, P. W., Kopple, K. D., & Mueller, L. (1990) *Biochemistry 29*, 7805−7813.
Kohda, D., & Inagaki, F. (1992a) *Biochemistry 31*, 677−685.
Kohda, D., & Inagaki, F. (1992b) *Biochemistry 31*, 11928−11939.
Koning, T. M. G., Boelens, R., & Kaptein, R. (1990) *J. Magn. Reson. 90*, 111−123.
Kraulis, P. (1991) *J. Appl. Crystallogr. 24*, 946−950.
Kumar, A., Ernst, R. R., & Wüthrich, K. (1980) *Biochem. Biophys. Res. Commun. 95*, 1−6.
Laskowski, R. A., MacArthur, M. W., Moss, D. S., & Thornton, J. M. (1993) *J. Appl. Crystallogr. 26*, 283−291.
Lee, J., & Wood, W. I. (1993) *Genomics 16*, 790−791.
Lemoine, N. R., Barnes, D. M., Hollywood, D. P., Hughes, C. M., Smith, P., Dublin, E., Prigent, S. A., Gullick, W. J., & Hurst, H. C. (1992a) *Br. J. Cancer 66*, 1116−1121.
Lemoine, N. R., Lobresco, M., Leung, H., Barton, C., Hughes, C. M., Prigent, S. A., Gullick, W. J., & Kloppel, G. (1992b) *J. Pathol. 168*, 269−273.
Levi, A. D., Bunge, R. P., Lofgren, J. A., Meima, L., Hefti, F., Nikolics, K., & Sliwkowski, M. X. (1995) *J. Neurosci. 15*, 1329−1340.
Lewis, G. D., Lofgren, J. A., McMurtrey, A. E., Nuijens, A., Fendly, B. M., Bauer, K. D., & Sliwkowski, M. X. (1995) *Cancer Res.* (submitted for publication).
Live, D. H., Davis, D. G., Agosta, W. C., & Cowburn, D. (1984) *J. Am. Chem. Soc. 106*, 1939−1941.
Ludvigsen, S., & Poulsen, F. M. (1992) *J. Biomol. NMR 2*, 227−233.
Marchionni, M. A., Goodearl, A. D. J., Chen, M. S., Bermingham-McDonogh, O., Kirk, C., Hendricks, M., Danehy, F., Misumi, D., Sudhalter, J., Kobayashi, K., Wroblewski, D., Lynch, C., Baldassare, M., Hiles, I., Davis, J. B., Hsuan, J. J., Totty, N. F., Otsu, M., McBurney, R. N., Waterfield, M. D., Stroobant, P., & Gwynnw, D. (1993) *Nature 362*, 312−318.
Marion, D., Driscoll, P. C., Kay, L. E., Wingfield, P. T., Bax, A., Gronenborn, A. M., & Clore, G. M. (1989a) *Biochemistry 28*, 6150−6156.
Marion, D., & Wüthrich, K. (1983) *Biochem. Biophys. Res. Commun. 113*, 967−974.
Marion, D., Ikura, M., & Bax, A. (1989b) *J. Magn. Reson. 84*, 425−430.
Marion, D., Ikura, M., Tschudin, R., & Bax, A. (1989c) *J. Magn. Reson. 85*, 393−399.
Marion, D., Kay, L. E., Sparks, S. W., Torchia, D. A., & Bax, A. (1989d) *J. Am. Chem. Soc. 111*, 1515−1517.
Messerle, B. A., Wider, G., Otting, G., Weber, C., & Wüthrich, K. (1989) *J. Magn. Reson. 85*, 608−613.
Meyer, D., & Birchmeier, C. (1994) *Proc. Natl. Acad. Sci. U.S.A. 91*, 1064−1068.
Modjtahedi, H., & Dean, C. (1994) *Int. J. Oncol. 4*, 277−296.
Molday, R. S., Englander, S. W., & Kallen, R. G. (1972) *Biochemistry 11*, 150−158.
Montelione, G. T., Winkler, M. E., Rauenbuehler, P., & Wagner, G. (1989) *J. Magn. Reson. 82*, 198−204.
Montelione, G. T., Wüthrich, K., Burgess, A. W., Nice, E. C., Wagner, G., Gibson, K. D., & Scheraga, H. A. (1992) *Biochemistry 31*, 236−249.
Moscoso, L. M., Chu, G. C., Gautam, M., Noakes, P. G., Merlie, J. P., & Sanes, J. R. (1995) *Dev. Biol. 172*, 158−169.
Moy, F. J., Li, Y.-C., Rauenbuehler, P., Winkler, M. E., Scheraga, H. A., & Montelione, G. T. (1993) *Biochemistry 32*, 7334−7353.
Mudge, A. W. (1993) *Curr. Biol. 3*, 361−364.
Nagata, K., Kohda, D., Hatanaka, H., Ichikawa, S., Matsuda, S., Yamamoto, T., Suzuki, A., & Inagaki, F. (1994) *EMBO J. 13*, 3517−3523.
Nilges, M., Clore, G. M., & Gronenborn, A. M. (1988) *FEBS Lett. 239*, 317−324.
Orr-Urtreger, A., Trakhtenbrot, L., Ben-Levy, R., Wen, D., Rechavi, G., Lonai, P., & Yarden, Y. (1993) *Proc. Natl. Acad. Sci. U.S.A. 90*, 1867−1871.
Peles, E., Bacus, S. S., Koski, R. A., Lu, H. S., Wen, D., Ogden, S. G., Ben-Levy, R., & Yarden, Y. (1992) *Cell 69*, 205−216.
Plateau, P., & Guéron, M. (1982) *J. Am. Chem. Soc. 104*, 7310−7311.
Plowman, G. D., Culouscou, J.-M., Whitney, G. S., Green, J. M., Carlton, G. W., Foy, L., Neubauer, M. G., & Shoyab, M. (1993a) *Proc. Natl. Acad. Sci. U.S.A. 90*, 1746−1750.
Plowman, G. D., Green, J. M., Culouscou, J.-M., Carlton, G. W., Rothwell, V. M., & Buckley, S. (1993b) *Nature 366*, 473−475.
Press, W. H., Flannery, B. P., Teukolsky, S. A., & Vetterling, W. T. (1986) *Numerical Recipes. The Art of Scientific Computing*, Cambridge University Press, Cambridge.
Rance, M. (1987) *J. Magn. Reson. 74*, 557−564.
Rance, M., & Byrd, R. A. (1983) *J. Magn. Reson. 54*, 221−240.
Rance, M., & Wright, P. E. (1986) *J. Magn. Reson. 66*, 372−378.
Rance, M., Sørensen, O. W., Bodenhausen, G., Wagner, G., Ernst, R. R., & Wüthrich, K. (1983) *Biochem. Biophys. Res. Commun. 117*, 479−485.
Reilly, D., & Fairbrother, W. J. (1994) *J. Biomol. NMR 4*, 459−462.
Robertson, A. D., & Baldwin, R. L. (1991) *Biochemistry 30*, 9907−9914.
Shaka, A. J., Barker, P. B., & Freeman, R. (1985) *J. Magn. Reson. 64*, 547−552.
Sliwkowski, M. X., Schaefer, G., Akita, R. W., Lofgren, J. A., Fitzpatrick, V. D., Nuijens, A., Fendly, B. M., Cerione, R. A., Vandeln, R. L., & Carraway, K. L., III (1994) *J. Biol. Chem. 269*, 14661−14665.
Srinivasan, N., Sowdhamini, R., Ramakrishnan, C., & Balaram, P. (1990) *Int. J. Pept. Protein Res. 36*, 147−155.
Tropp, J. (1980) *J. Chem. Phys. 72*, 6035−6043.
Tzahar, E., Levkowitz, G., Karunagaran, D., Yi, L., Peles, E., Lavi, S., Chang, D., Liu, N., Yayon, A., Wen, D., & Yarden, Y. (1994) *J. Biol. Chem. 269*, 25226−25233.
Vuister, G. W., & Bax, A. (1993) *J. Am. Chem. Soc. 115*, 7772−7777.
Vuister, G. W., Boelens, R., & Kaptein, R. (1988) *J. Magn. Reson. 80*, 176−185.
Vuister, G. W., de Waard, P., Boelens, R., Vliegenthart, J. F. G., & Kaptein, R. (1989) *J. Am. Chem. Soc. 111*, 772−774.
Vuister, G. W., Boelens, R., Padilla, P., Kleywegt, G. J., & Kaptein, R. (1990) *Biochemistry 29*, 1829−1839.
Wagner, G., Braun, W., Havel, T. F., Schaumann, T., Go, N., & Wüthrich, K. (1987) *J. Mol. Biol. 196*, 611−639.
Wallasch, C., Weiss, F. U., Niederfellner, G., Jallal, B., Issing, W., & Ullrich, A. (1995) *EMBO J. 14*, 4267−4275.
Weiner, S. J., Kollman, P. A., Case, D. A., Singh, U. C., Ghio, C., Alagona, G. S., Profeta, J., & Weiner, P. (1984) *J. Am. Chem. Soc. 106*, 765−784.
Weiner, S. J., Kollman, P. A., Nguyen, D. T., & Case, D. A. (1986) *J. Comput. Chem. 7*, 230−252.
Wilmot, C. M., & Thornton, J. M. (1988) *J. Mol. Biol. 203*, 221−232.
Wishart, D. S., Sykes, B. D., & Richards, F. M. (1992) *Biochemistry 31*, 1647−1651.
Wüthrich, K. (1986) *NMR of Proteins and Nucleic Acids*, John Wiley & Sons, Inc., New York.
Wüthrich, K., Billeter, M., & Braun, W. (1983) *J. Mol. Biol. 169*, 949−961.
Yip, P. (1990) *J. Magn. Reson. 90*, 382−383.
Zhao, D., & Jardetzky, O. (1994) *J. Mol. Biol. 239*, 601−607.
Zuiderweg, E. R. P., Boelens, R., & Kaptein, R. (1985) *Biopolymers 24*, 601−610.

BI952626L